7-19-2013

Computer Simulations of Nanorods Interaction With Lipid Membrane

Niraj Shrestha

COMPUTER SIMULATIONS OF NANORODS INTERACTION WITH LIPID MEMBRANE

by

Niraj Shrestha

A Thesis

Submitted in Partial Fulfillment of the

Requirements for the Degree of

Master of Science

Major: Physics

The University of Memphis

August 2013

ACKNOWLEDGEMENT

When I joined the research group of Dr. Mohamed Laradji, I had very little knowledge of programming and computational work. In that regard, I would like to express my gratitude to Dr. Laradji for being patient with my programming knowledge and guiding me in my research work. His guidance provided me with the confidence to continue my work with resilience when I found obstacles and doubts in my path. Ultimately, it culminated in the completion of this work, which I am proud of. I would also like to thank my research partner Eric John Spangler for helping me out with numerous problems that I faced during my time with Dr. Laradji's group. His mastery of programming languages and understanding of the research work are impeccable. He is always there to lend me a hand whenever I faced problems, whether small or big, with my research work and I am very grateful to him for all his support. I am very fortunate to have a research partner like him. I would also like to express my gratitude to Ibrahim Souki, who like Eric, was always there to help me whenever I came across problems regarding simulations and computer clusters. His genuine interest to make things clear and explain things in great detail were godsend.

Finally, I would like to thank the Physics department for all their support and encouragement during my two years of stay at this University.

ABSTRACT

Shrestha, Niraj. M.S. The University of Memphis. August 2013. Computer Simulations of Nanorods Interaction with Lipid Membrane. Major Professor: Mohamed Laradji, Ph.D.

Analyzing the interaction between the lipid membranes and nanoparticles helps to determine beneficial and harmful effects of nanoparticles on cells. Since the point of entry of cells is their plasma membrane, interactions between nanorods and lipid membranes were studied using molecular dynamics simulations. The effect of nanorods on membrane morphology was investigated systematically as a function of nanorods interaction with the lipid membrane, their surface coverage and number surface density. Our results indicate that when adsorbed on the membrane, the nanorods may cluster into chains and may lead to strong membrane deformations due to curvature driven interaction between nanorods. At particular nanorod-lipid interaction, single nanorod internalizes into the membrane via endocytosis. This happens to minimize the energy cost due to high bending of the membrane. At high nanorods' density and large nanorods' size, it was found that the nanorods lead to membrane lysis which can be attributed to high surface coverage of nanorods.

TABLE OF CONTENTS

LIST OF FIGURES

CHAPTER 1

INTRODUCTION

1.1 Nanotechnology at a Glance

Nanotechnology is a technique by which people operate matter on its atomic level. At this level of matter, properties of materials vary significantly from their bulk counterparts.[1] For example, it is reported that zinc oxide nanoparticles have superior blocking action against UV radiation as compared to its bulk substitute. Therefore, it is frequently used in synthesizing sunscreen lotions.[2] Nanoparticles have large surface area-to-volume ratio than bulk materials. Because of this and their small size, they are capable of penetrating the cell membrane.[1,3] The surface area to volume ratio has great significances in living organisms. The small size of the cells ensures quick diffusion of necessary materials like nutrients and oxygen which are essential for the survival of the cell.[4] Nanoparticles' size are comparable to those of biological materials like proteins etc. and have the ability to cross barriers of different cell organelles because of their large area to volume ratio.[1] The interaction of nanoparticles with cells may depend on their dose, their ability to disperse within the body and their solubility.[1] Hence, understanding of how nanoparticles interact with cell is warranted. Thus, nanotechnology is becoming an area of intense scientific research in the field of biomedical science.

1.2 Beneficial Applications of Nanotechnology in Medical Sciences

Nanotechnology has wide applications in medical science. The high surface area to volume ratio of nanoparticles allows various functional groups to be adhered to their surface that can then easily track and bind to targeted cells.[5] Thus, nanoparticles can be used for targeted drug delivery,[6] fluorescent biological labels,[7] and diagnosis of

pathologies at early stages.[8] This targeted drug delivery technology can be used for faster cure of diseases with little side effects compared to other drugs.[6] In addition, investigation of nanoparticles for gene delivery purpose is underway. Gene transfer was practiced in vitro and in vivo with different kind of nanoparticles.[9] It has been found that gene transfer can be accomplished with very low cell toxicity with silica nanoparticles of size~40 nm.[9] Nowadays, in biomedicine, nanotechnology research is mainly focused on tissue regeneration, bone renovation, immunity and has even brought new hope to cancer and other disease treatment.[10] For instance, three magnetic, iron-oxide nanospheres chemically linked to one doxorubicin-loaded liposome were found to cure breast cancer.[11] Nano treatment reduces the dose of doxorubicin and therefore is less toxic.[11] The study of endocytosis of gold NPs with different sizes (45 nm, 70 nm and 110 nm) in various cells (the human cancer cell line such as, CL1-0 and HeLa) is also reported.[12] From the study of the 3-Dimensional distributions of gold NPs, size dependent endocytosis of gold NPs is experimentally verified. It has been found that gold NPs of diameter 45 nm are the most efficient in terms of composition and size in targeted drug delivery technique.[12] Besides these, metal-based nanoparticles can be used as antimicrobial agent against common pathogenic microorganisms. Silver nanoparticles of size ~16 nm with concentration as low as 60 μg/ml have been found to stick to the cell wall of the E. coli and penetrate the cell membrane causing complete cytoxicity.[13] The application of nanotechnology is in progress. Since the toxic effect of nanoparticles is reported, knowledge about the interactions between nanoparticles and biological systems is momentous to move nanotechnology towards biomedical applications.[14]

1.3 Potential Hazards of Nanoparticles on Environment and on Human Health

The study of potential risks of engineered nanoparticles to human health and environment is underway. Nanoparticles may discharge into the environment through waste streams from industrial plants.[1,15] Accidental releases of nanoparticles into river and atmosphere also may happen during the production and transportation of their products.[1,15] There is a lack of information regarding nanoparticles' emission into the environment. Regarding nanoparticles' impact on human health, the level of danger and destruction associated with their interaction with living cells is still unclear. Thus, attention must be paid on every possibility including toxic effects of nanoparticles' to the environment and living beings.

The plasma membrane is the entry point of cells. Because of their nanoscale size, nanoparticles can translocate from these entry portals to anywhere in the body. They may easily disperse in the bloodstream, penetrate vital organs like lungs, kidneys etc.[1] Nanoparticles may cause irreversible destruction to living cells by oxidative stress and organelle injury as well.[1] However, their toxicity depends on factors including size, composition, surface chemistry and surface coating.[1] Carbon nanotubes have been found to cause lung irritation, chronic lung inflammations and exacerbation of asthma.[16] Studies have also shown that sometimes reactive oxygen species may be formed on the surface of some nanoparticles that may have harmful effect on human health. Reactive oxygen species have been found to damage DNA that ultimately leads to lung cancer.[17] Cytotoxicity that depends upon geometry is also reported. Carbon nanotubes, being hydrophobic, interact with hydrophobic regions of cell membranes and internalize into the cell via endocytosis. These carbon nanotubes are then wrapped by DNA causing cell

death.[18] Although, it may be too early to say whether nanoparticles are toxic or not, the current observed results suggest that proper study of the potential risks of nanotechnology is required to minimize its harmful impacts on human health.

1.4 Lipid Membranes

Many of the biological processes like cellular transport, neural functions and enzymatic activities either occur in the plasma membrane or are mediated by it. These processes are governed by physical principles and that is why both physicists and chemists have been very interested in studying lipid membranes during the last few decades.[19] The plasma membrane is a surface that encapsulates a cell. The main component of the plasma membrane is a thin layer of self-assembled lipids and proteins and it is typically around 5 nm thick. The stability of the plasma membrane, as well as other membranes inside the cell, is provided by a unique molecular structure of lipids. A lipid molecules is composed of two parts - (1) a hydrophilic part that is either ionic or polar and prefers an aqueous environment, and (2) a hydrophilic part composed in general of two hydrocarbon tail groups that are apolar and therefore hates to be surrounded by water molecules. Due to this anisotropic structure of lipids, they rapidly self-assemble into bilayers when mixed with water as shown in figure 1.4.1. This self-assembly is mediated by the repulsive hydrophobic interactions between the lipids hydrocarbon tails and water molecules, leading to the arrangement of the lipids into a bilayer such that the tails are completely shielded from water.[20] Due to the apolar nature of the hydrocarbon tails, lipid membranes act as barriers to ions and other water-soluble substances. The lipid bilayer is in a solid (gel) phase at low temperatures and undergoes a phase transition to a fluid phase at higher temperatures.[21] Biological membranes are in

the fluid phase due to the high amount of unsaturated lipids and cholesterol. Fluid membranes allow transport of a variety of transmembrane proteins that are essential for a myriad of physiological functions. Fluid membranes can also easily deform and therefore allow for processes that necessitate membrane deformation such as cytokinesis, endocytosis, apoptosis, and cell motility.

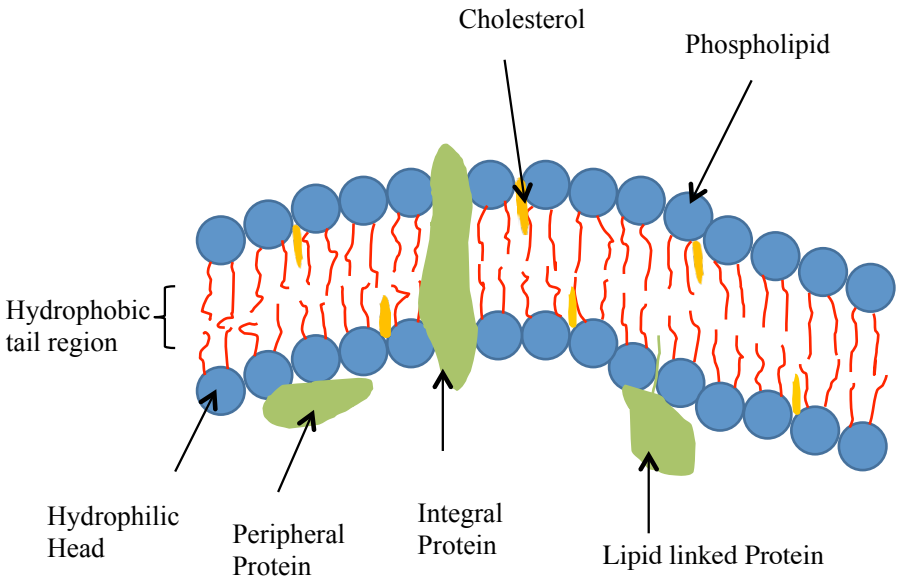

Figure 1.4.1. Schematic diagram showing lipid bilayer in biological membrane.

1.5 Objectives

It has been established experimentally that in some circumstances, nanoparticles interacting with lipid membranes lose their integrity and form pores in the membrane. Experimentally, it is observed that when polar silica nanoparticles of size 1.2 – 22 nm, deposited on mica surface, interacted with L-α-dimyristoyl phosphatidylcholine lipid

membrane, they formed pores.[22] Computer simulation results of pore formation in the membrane have also been reported for hydrophobic nanoparticles.[23] In addition, various molecular dynamics simulations have been carried out to understand the internalization pathways of nanoparticles into the cell. Surface chemistry is reported to play an important role in this process. Nanoscale pores might be linked to nanoparticles low charge densities while endocytosis phenomenon might be associated with nanoparticles with higher charge density.[24] It has been observed, by coarse-grained molecular dynamics simulations, that electrostatic attractive force facilitates the adherence of a charged nanoparticle to the lipid membrane.[25] A charged NP is found to be wrapped completely by the lipid membrane as the electrostatic force is increased.[25] Charged NP adhering to a membrane is also found to cause a local transition in fluid bilayers.[25]

In all of the cases describe above, focus was concentrated on the interactions between nanospheres and hydrophobic (water hating) nanorods with lipid membranes. My computational research studies the interactions of hydrophilic (water loving) nanorods and the lipid membrane with the help of "Implicit-solvent mesoscale model based on soft-core potentials for self-assembled lipid membranes".[21] This research is particularly focused on understanding: (a) how nanoparticles affect the structural and mechanical properties of lipid membranes? (b) Do nanoparticles affect the stability of lipid membrane? Particularly, can they lead to lysis of cells? (c) How are nanoparticles internalized in the cell? In particular, are they internalized through endocytosis or through a pore? (c) How do the properties of nanoparticles like their interactions with lipid, size, shape and density affect lipid membranes and the internalization process? Thus, in this study, we aim to investigate systematically the effects of nanorods on lipid membranes'

morphology and stability as a function of nanorods interaction with lipids, aspect ratio, size and their surface coverage. In my simulations, linear cluster of nanorods is observed at higher values of nanorod-lipid head interactions and at higher lipid density of bilayer as well. It is also observed that a single nanorod internalizes into the cell via endocytosis at particular nanorod-lipid head interaction. We also found endocytosis of nanoparticles depending on their dimensions and interactions with the lipid head groups. Finally, under certain circumstances, pores are also observed to form in the vicinity of the nanoparticles. These pores can be short-lived or may eventually lead to instability of the lipid bilayer.

Chapter 2

Model and Numerical Approach

2.1 Lipid Membranes Model

In this model, a coarse-grained model of lipids is used, where groups of atoms are integrated into soft beads. Lipid molecules are considered to be semiflexible amphiphilic chains consisting of one hydrophilic head and two hydrophobic tails.

Here, the interaction potential between particles consists of three contributions: harmonic interactions for the bonds in the lipid chain (U_{bond}), three body interactions to ensure bending rigidity (U_{bend}) and two body interaction between neighboring beads (U_o).[21,26] Hence,

$$U(r_i)= \sum_{i,j} U_o\left(r_{i,j}\right)+ \sum_i U_{bond}\left(r_{i,i+1}\right)+ \sum_i U_{bend}(r_{i-1}, r_i, r_{i+1}) \qquad (2.1.1)$$

The **soft pairwise interaction** between two beads is given by,[21,26]

$$U_o(r)= \begin{cases} \left(U^{\alpha\beta}_{max}- U^{\alpha\beta}_{min}\right) \frac{(r_m-r)^2}{r^2}+ U^{\alpha\beta}_{min} & \text{if } r \le r_m \\ -2U^{\alpha\beta}_{min} \frac{(r_c-r)^3}{(r_c-r_m)^3}+3U^{\alpha\beta}_{min} \frac{(r_c-r)^2}{(r_c- r_m)^2} & \text{if } r_m < r \le r_c \\ 0 & \text{if } r > r_c \end{cases} \qquad (2.1.2)$$

where, r_m=equilibrium distance between beads and r_c= cut of distance.

Since a mesoscale-implicit solvent model based on soft-core potentials is used, the self-assembly of lipid molecules into a bilayer results from an effective attractive interaction

between the tail particles. In this model, $U_{min}^{\alpha\beta} = 0$, if α or β = head particle, $U_{min}^{\alpha\beta} < 0$, if α = β = tail particle and $U_{max}^{\alpha\beta} > 0$ for any values of α or β.

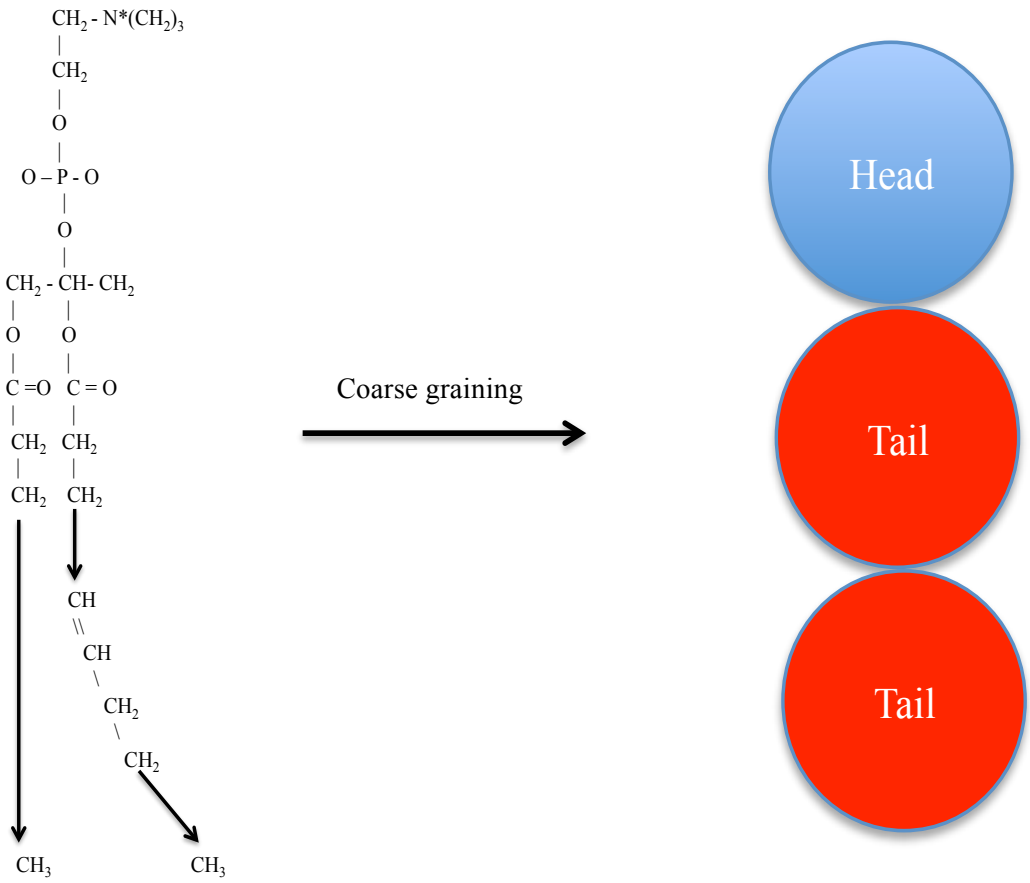

Figure 2.1.1. A schematic diagram showing how a phosphatidylcholine lipid is coarse-grained into a chain of beads.

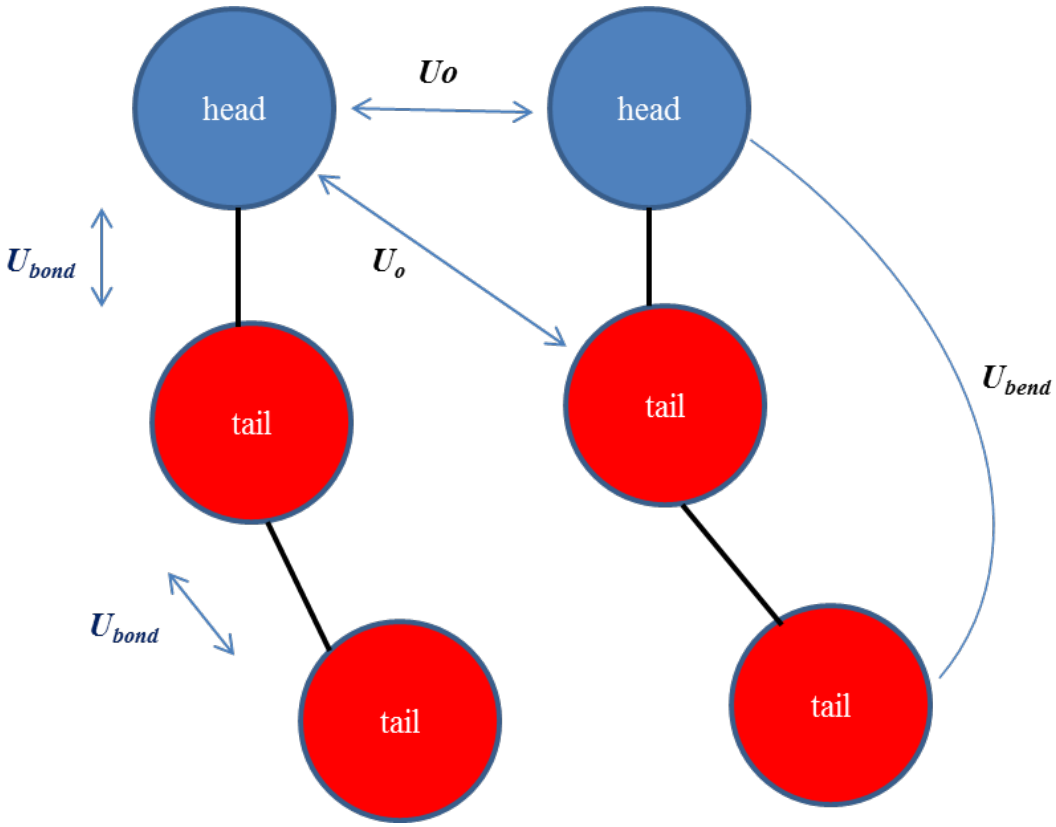

Figure 2.1.2. The three types of interactions used in our model.

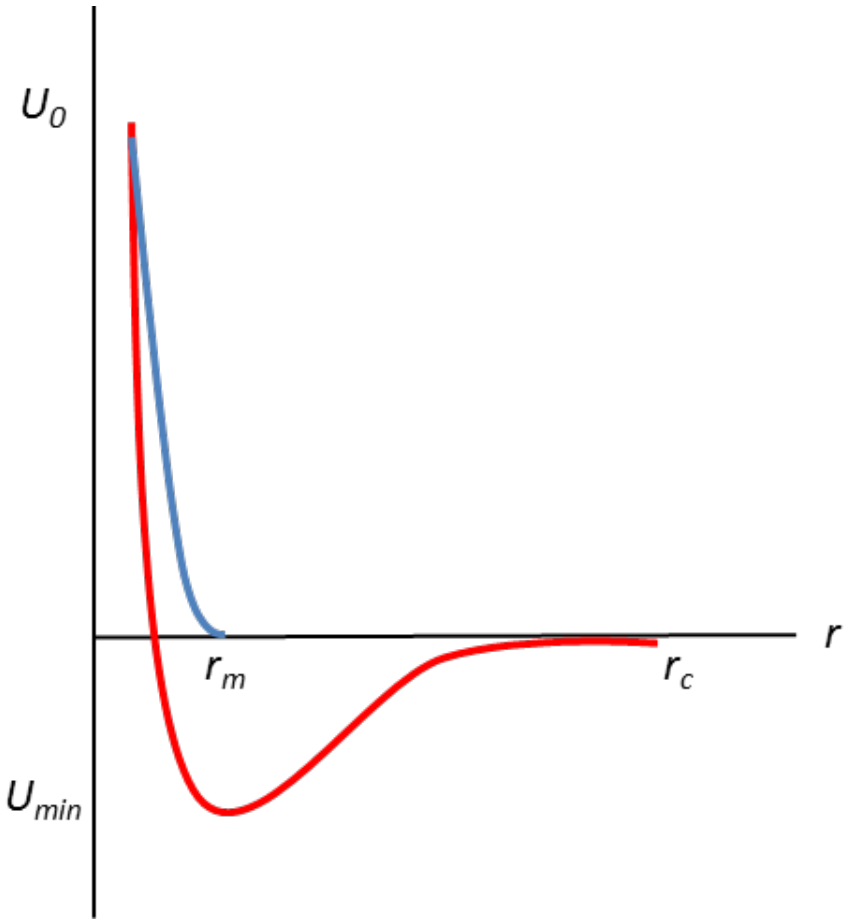

Figure 2.1.3. Soft two-body interaction between particles (blue line for head-head or head-tail interaction while red line for tail-tail interaction).

The **harmonic interaction of bond (U_{bond})** helps to connect monomers in a lipid chain and is given by,[21,26]

$$U^{\beta}_{bond}(r)=k^{\beta}_{bond}\left(r-a_b\right)^2 \qquad (2.1.3)$$

where k^{β}_{bond} is bond rigidity constant and a_b is bond length.

The **three body interaction (U_{bend})** accounts for bending rigidity of lipid molecules is,[21,26]

$$U_{bend}^{\beta}=\frac{1}{2}\, k_{bend}^{\beta}\left(\cos\theta_o-\cos\theta_i\right)^2 \qquad (2.1.4)$$

where k_{bend}^{β} is bending rigidity constant of a chain, $\theta_o=180^o$ and $\cos\theta_o=(\mathbf{r}_{i,i-1}.\mathbf{r}_{i,i+1}/r_{i,i-1}.r_{i,i+1})$.

2.2 Nanorod Model

In this research, nanoparticles are constructed from aggregating small beads (similar to those used for the lipid head or tail particles). The beads in a nanoparticles are arranged in a face-centered-cubic lattice and are connected to each other via stiff harmonic springs. The primitive lattice vectors of FCC lattice system are given as

$$a_1 = (½)\, a\,(0,1,1), \quad a_2 = (½)\, a\,(1,0,1) \quad \text{and} \quad a_3 = (½)\, a\,(1,1,0) \qquad (2.2.1)$$

where 'a' is lattice constant. In this model, a = 0.5 nm

Here, nearest neighbor distance = $a/[2]^{½}$ = 0.3535 nm (approx.)

Figure 2.2.1. Nanorod (D = 2.76 nm, H = 13.80 nm)

2.3 Molecular Dynamics

Molecular dynamics is a powerful simulation tool used to study both equilibrium and dynamic properties of a variety of systems including nanoparticles, lipid membranes etc. Molecular dynamics provide a very close description of systems at a microscopic level. In molecular dynamics simulations, particles are moved according to Newton's laws of motion while in contact with a heat bath that allows the system to reach thermal equilibrium. With the trajectory of the particles' configurations, various thermodynamic quantities can be studied.[27]

Although, this method was originally developed for theoretical physics, it is now a very powerful tool in condensed matter physics, materials science, polymer science, biochemistry, and biophysics.

2.4 Numerical Approach

In present model, molecular dynamics with a Langevin thermostat is used to move the particles.[21,28] The equations of motion of particles, each having mass m, are given by

$$\frac{d\mathbf{r}_i(t)}{dt} = \mathbf{v}_i(t) \qquad (2.4.1)$$

$$m\frac{d\mathbf{v}_i(t)}{dt} = -\nabla_i U - \Gamma \mathbf{v}_i(t) + W_i(t) \qquad (2.4.2)$$

where , Γ : coefficient of bead's friction = $\sqrt{6}$ (m/ τ)

W: random force provided from thermal bath

The random force originating from thermal bath satisfies following correlation,

$$\langle \mathbf{W}_i(t) \rangle = 0 \qquad (2.4.3)$$

$$\langle \mathbf{W}_i(t) | \mathbf{W}_j(t') \rangle = 6\, k_B T\, \Gamma \delta_{i,j}\, \delta(t-t') \qquad (2.4.4)$$

The random force is derived from the thermal motion of molecules present in particles i and j. On the other hand, dissipative force is the result of friction between these particles. Random force always keeps the system in thermal motion. Dissipative force and random force together act as a thermostat. These pairs of forces ensure conservation of momentum locally which is a required property for a correct description of fluid hydrodynamics. Once the particle-particle interactions energy is provided, there are various algorithm techniques to integrate equations of motion. In the current simulations, the velocity-Verlet method is used for integrating equations of motions .[29,30]

2.5 Simulation Details and Parameter Selection

In this model, physical parameters like time (τ), length (r_m) and energy (ϵ) are considered as suitable units.[21,26] Time scale is given by

$$\text{Time } (\tau) = r_m \left(\frac{m}{\epsilon}\right)^{\frac{1}{2}} \qquad (2.5.1)$$

Thickness of bilayer in this model is $4.1r_m$. The estimated length scale is about, $r_m \approx 1$ nm and estimated time scale is about, $\tau \approx 1$ - 10 ns. This time scale is much larger than dissipative particle dynamics ($\tau \approx 0.1$ ns) that is why this model was chosen for my simulations. Many of our simulations are done at $k_BT = 3\epsilon$ and run for 100000 τ – 200000 τ. These are performed at constant area of lipid membrane and at constant pressure. Simulations are continued until an equilibrium state is reached. Initially, lipid bilayer is placed in a box of dimension $L_x \times L_y \times L_z$ with $L_x = L_y = L_z$. Periodic boundary conditions are also imposed in three directions [15, 20]. In this model, repulsive interaction is set up between nanorods and also between nanorods and lipid tails. On the other hand, attractive interaction is set up between nanorods and lipid heads. Thus, simulations are performed at different values of attractive interaction ($|U_{min}^{nh}| = 0.7\ \epsilon – 2.0\ \epsilon$) between nanorods and lipid heads. Simulations are done at different surface number densities of lipid bilayer too. Given below are the values of interactions set up between the particles in our simulations (h= head, t = tail and n = nanorod):

$U_{max}^{hh} = U_{max}^{th} = U_{max}^{nt} = 100\ \epsilon$, $U_{min}^{hh} = U_{min}^{th} = U_{min}^{nt} = 0$, $U_{min}^{tt} = -6\ \epsilon$,

$U_{max}^{nn} = U_{max}^{nh} = 200\ \epsilon$, $U_{min}^{nn} = 0$, $k_{bond}^{h} = k_{bond}^{t} = 100\ \epsilon/r_m^2$ $k_{bond}^{n} = 2600\ \epsilon/r_m^2$

$k_{bend}^{t} = 100\ \epsilon$, $a_b = 0.3535\ r_m$, $L_x = L_y = L_z$

Chapter 3

Results and Discussions

3.1 Linear Aggregation of Nanorods Mediated by Membrane

In this research, both constant area simulation and constant pressure simulation are done with 1, 7 and 20 nanorods. At constant area simulations (e.g. lipid density of 3.048/nm^2) of 20 thinner nanorods (e.g. D = 2.76 nm, H = 5.52 nm), clustering is observed with increase in nanoparticle-lipid head interaction from low to moderate value (at $|U_{min}| = 1.3\varepsilon$) as shown in figures 3.1.1.These types of clustering are also observed with 7 thinner nanorods (D = 2.76 nm, H = 5.52 nm) and (D = 2.76 nm, H = 13.80 nm) in the same condition as shown in figure 3.1.2 and figure 3.1.3 respectively. This result suggests that with increase in nanoparticles-lipid head interaction, local deformations on membrane increases. Thus, in order to reduce the curvature energy cost of bending the membrane due to these deformations, nanoparticles cluster into a chain. Nanorods clustering is also observed at higher lipid density (3.18 lipid/nm^2) i.e. at low membrane tension as shown in figures 3.1.4 – 3.1.6. With increase in lipid density, membrane becomes more flexible and can therefore deform more significantly when it interacts with nanoparticles which may in turn enhance clustering. This result is in agreement with the observations found by A. Saric and A. Cacciuto where they performed computational simulation study of spherical nanoparticles as a function of membrane bending rigidity.[31] They observed linear aggregation for biologically relevant values of bending rigidity. In order to ensure that equilibrium has been reached, time evolution of average local distance of nanorod from the membrane is examined as in figure 3.1.7- 3.1.10. Figures 3.1.11- 3.1.13 show that nanorod-lipid head interactions strongly affect the nanorod

wrapping by lipid membrane. In contrast to constant area simulations, constant pressure simulations show relatively significant deformation of membrane, which in turn mediates linear clustering as shown in figures 3.1.14 – 3.1.16. To ensure that the system has reached equilibrium, time evolution of area of lipid membrane is plotted as in figure 3.1.17. In these simulations, nanorods are also found to be wrapped by the membrane depending upon the strength of nanorod-lipid head interaction that is shown in figure 3.1.18.

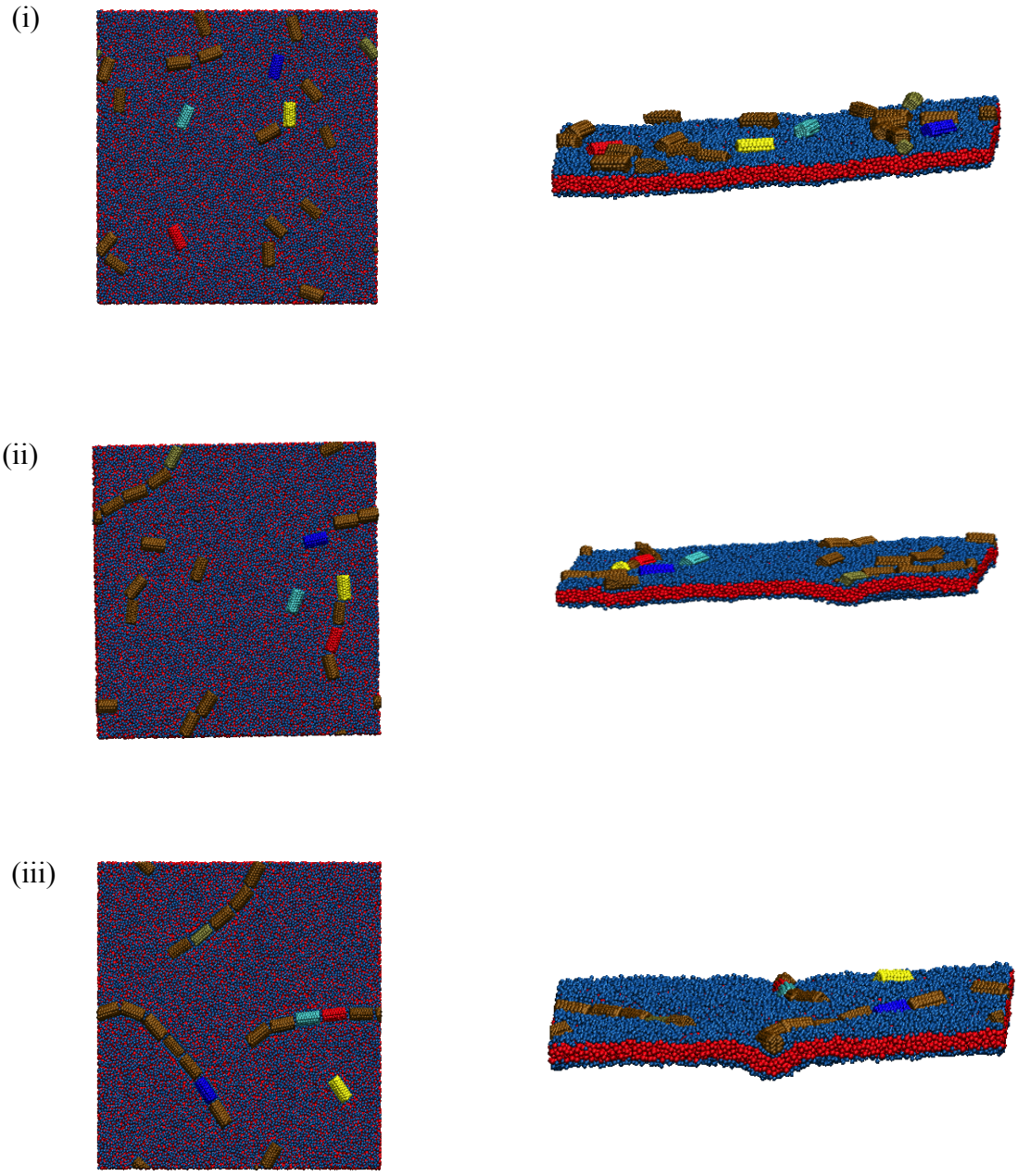

Figure 3.1.1. Snapshot of different view of 20 nanorods (D = 2.76 nm, H = 5.52 nm) interacting with membrane at (i) |Umin| = 0.7ε (ii) |Umin| = 1.0ε and (iii) |Umin| = 1.3ε.

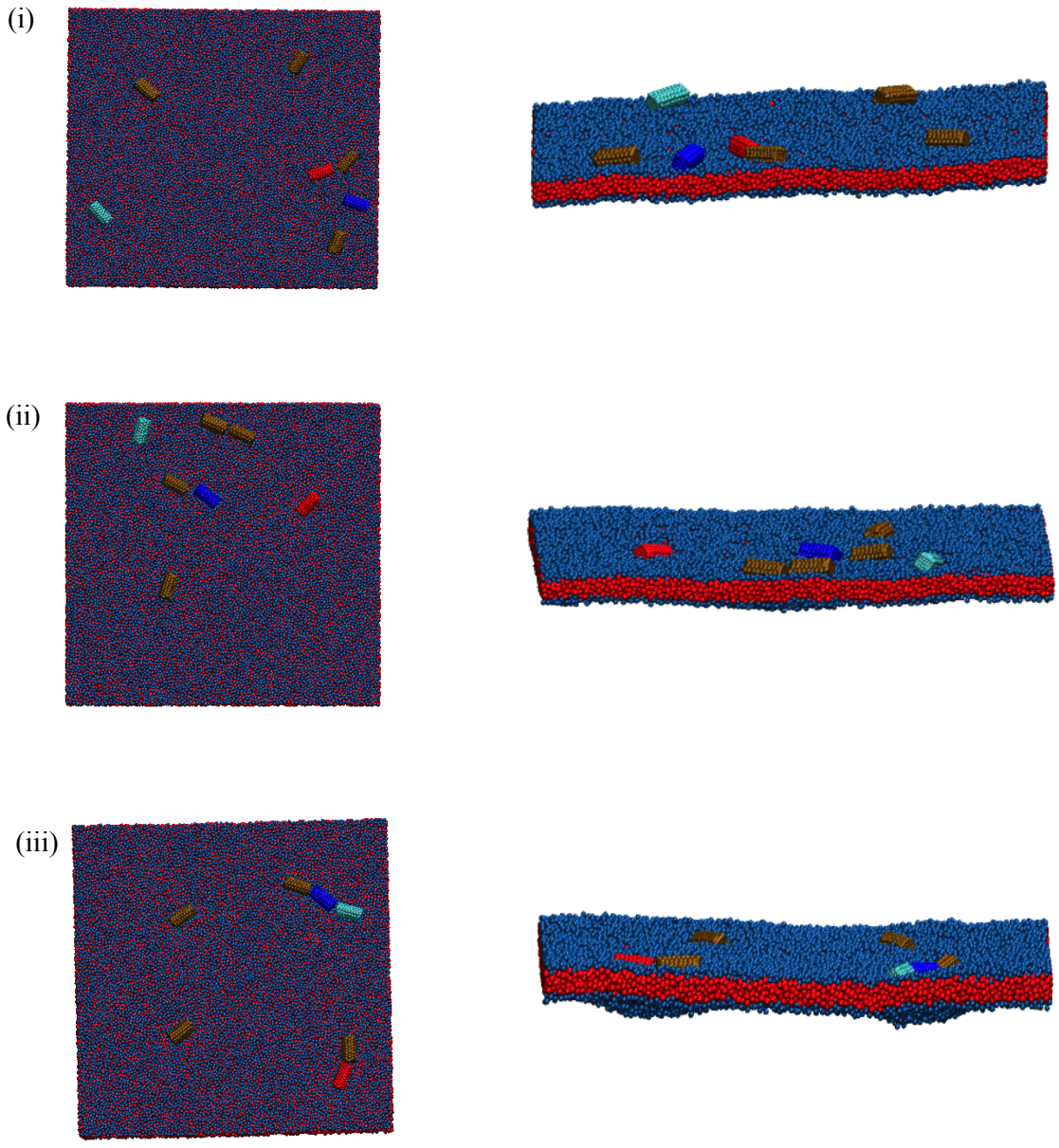

Figure 3.1.2. Snapshot of different view of 7 nanorods (D = 2.76 nm, H = 5.52 nm) interacting with membrane at (i) |Umin| = 0.7ε (ii) |Umin| = 1.0ε and (iii) |Umin| = 1.3ε [lipid density = 3.048 lipid/nm2].

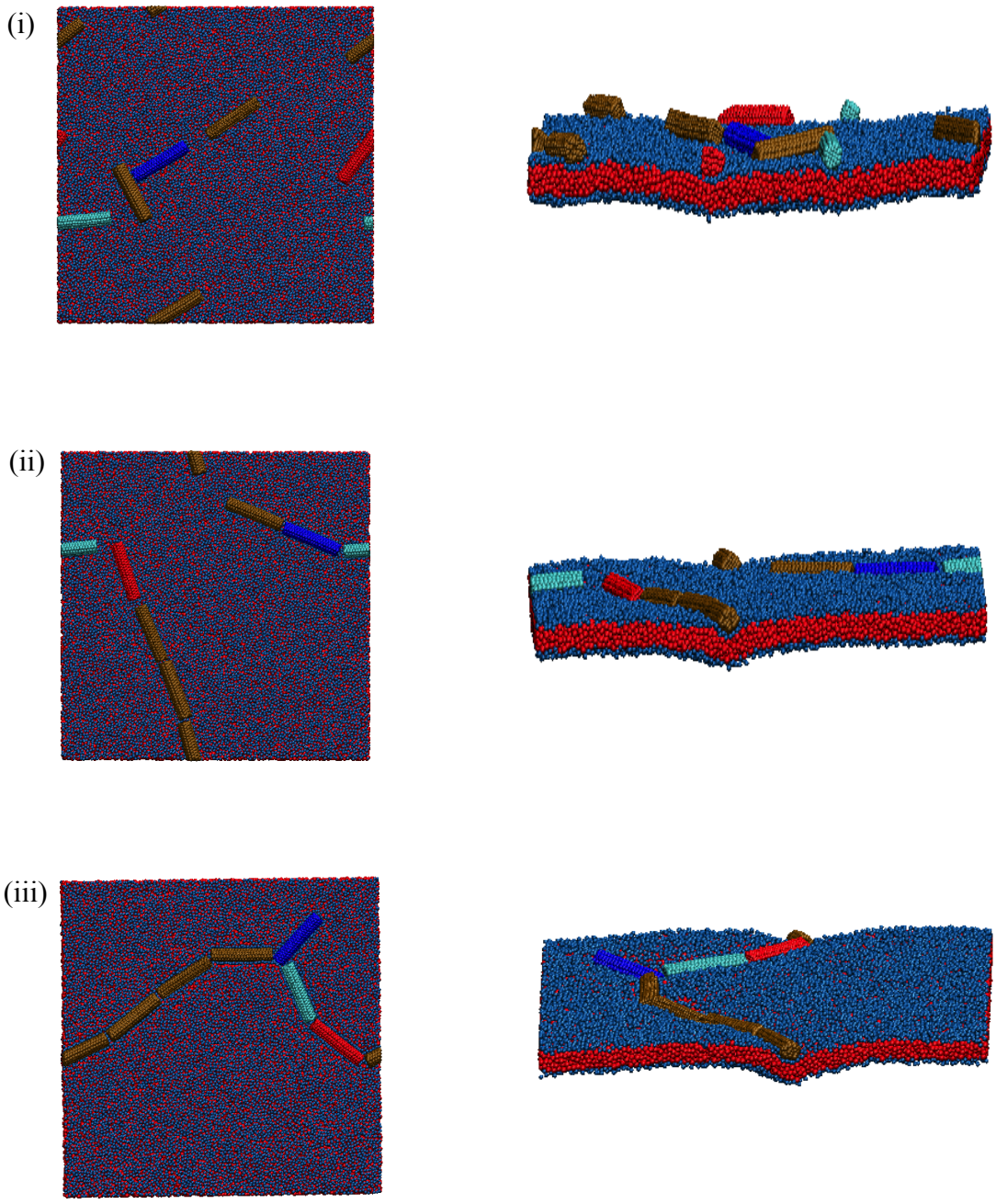

Figure 3.1.3. Snapshot of different views of 7 nanorods (D = 2.76 nm, H = 13.80 nm) interacting with membrane at (i) $|U_{min}| = 0.7\varepsilon$ (ii) $|U_{min}| = 1.0\varepsilon$ and (iii) $|U_{min}| = 1.3\varepsilon$ [lipid density = 3.048 lipid/nm^2].

(i)

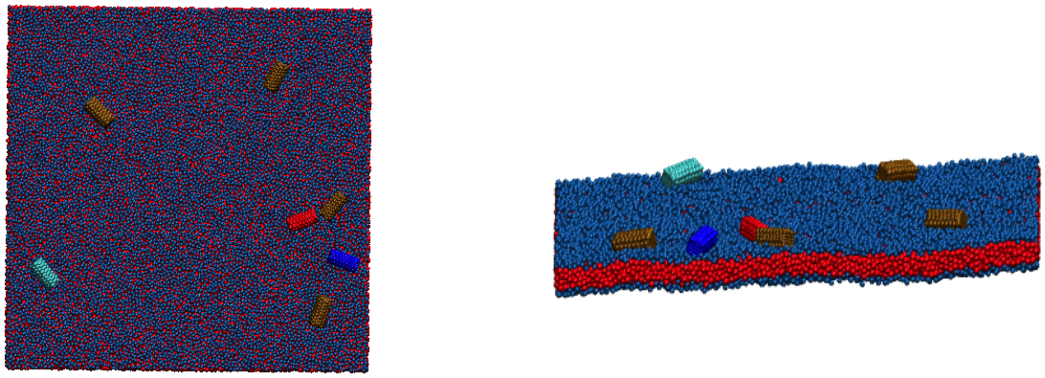

(ii)

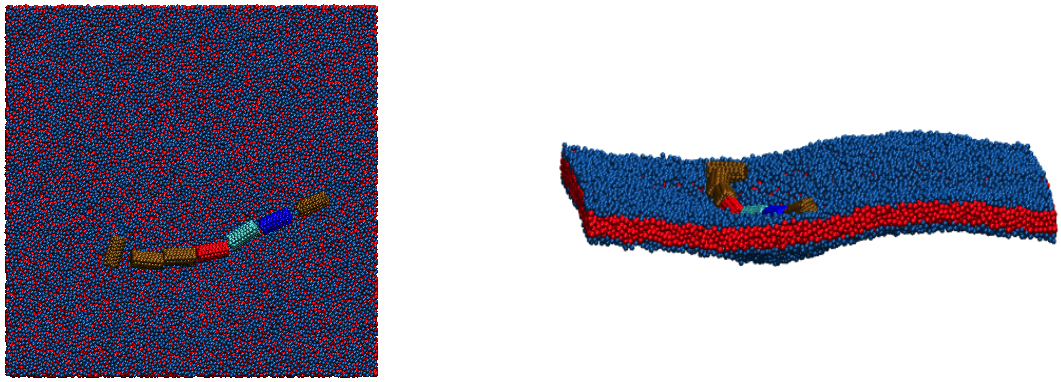

Top View Lateral View

Figure 3.1.4. Snapshot of different views of 7 nanorods (D = 2.76 nm, H = 5.52 nm) interacting with membrane at $|U_{min}| = 0.7\varepsilon$ when (i) lipid density = 3.048 lipid/nm^2 and (ii) lipid density = 3.180 lipid/nm^2.

(i)

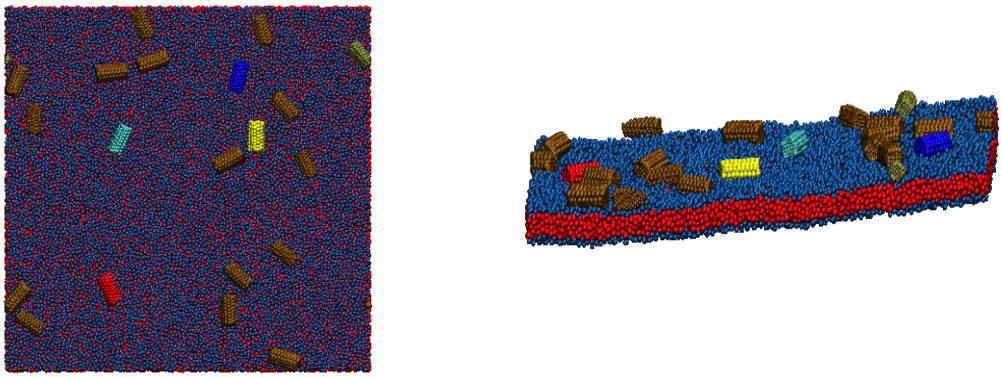

(ii)

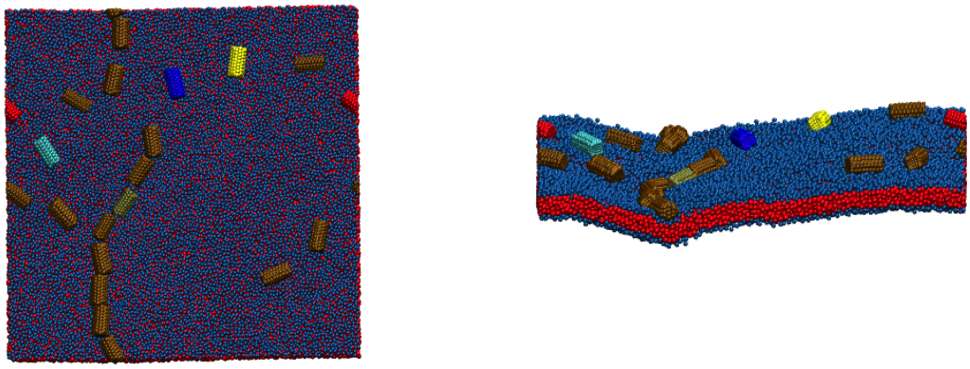

Top View Lateral View

Figure 3.1.5. Snapshot of different views of 20 nanorods (D = 2.76 nm, H = 5.52 nm) interacting with membrane at $|U_{min}| = 0.7\varepsilon$ when (i) lipid density = 3.048 lipids/nm^{2}and (ii) lipid density = 3.180 lipids/nm^2.

(i)

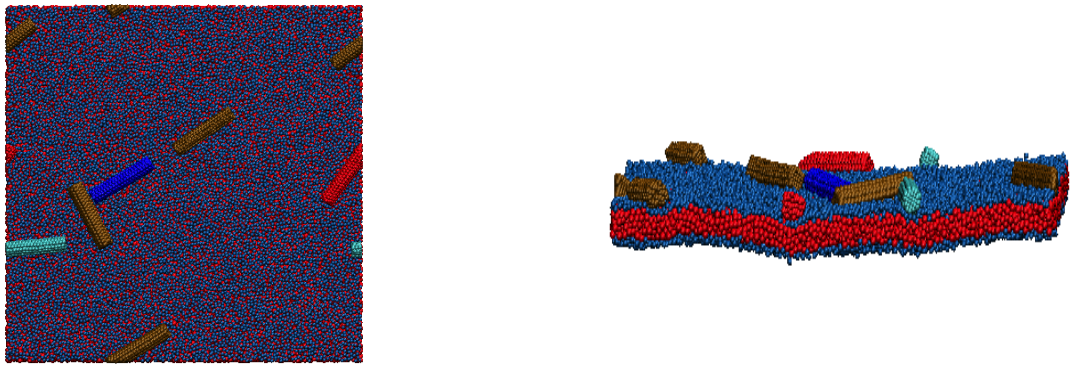

(ii)

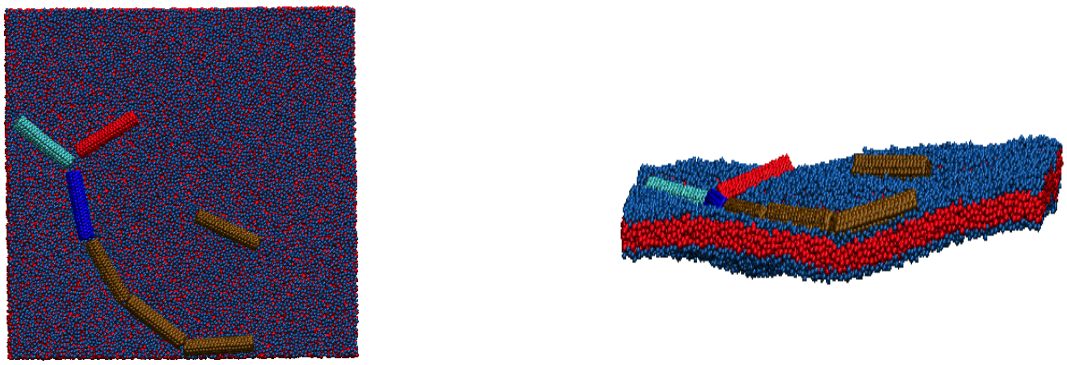

Top View Lateral View

Figure 3.1.6. Snapshot of different views of 7 nanorods (D = 2.76 nm, H = 13.80 nm) interacting with membrane at $|U_{min}| = 0.7\varepsilon$ when (i) lipid density = 3.048 lipids/nm^{2}and (ii) lipid density = 3.180 lipids/nm^2.

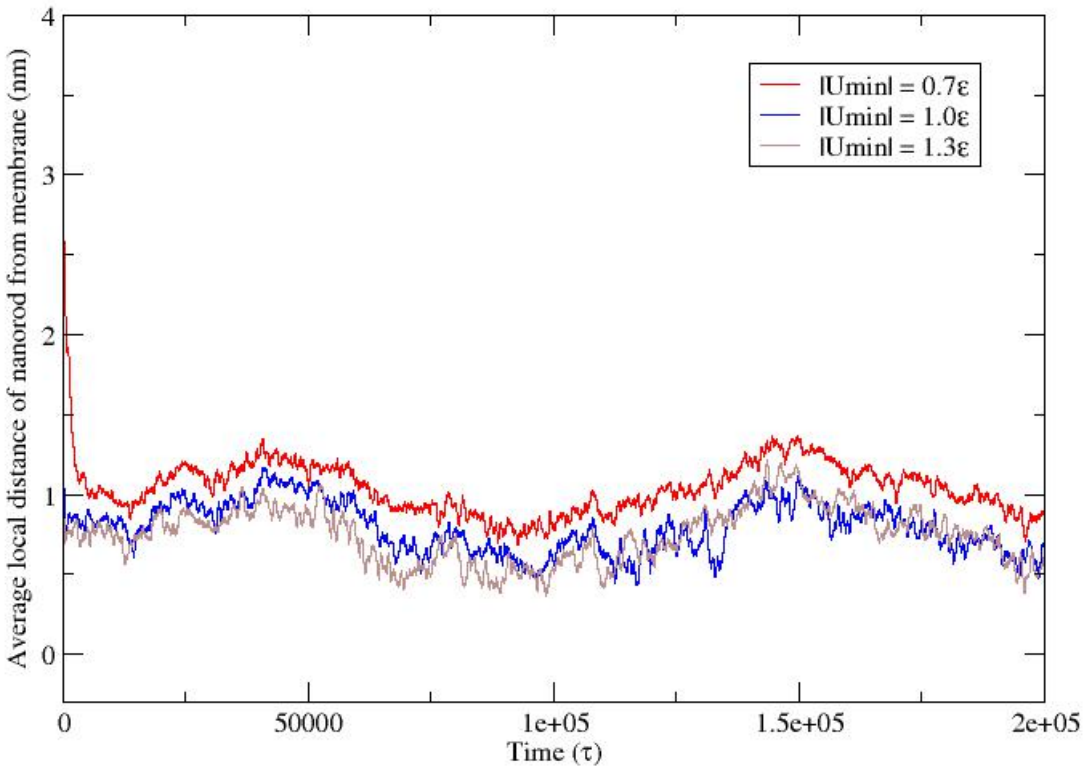

Figure 3.1.7. The time evolution of average local distance between nanorods and lipid membrane at constant area simulation of 20 nanorods (D = 2.76 nm, H = 5.52 nm) interacting with membrane at (i) $|U_{min}| = 0.7\varepsilon$ (ii) $|U_{min}| = 1.0\varepsilon$ and (iii) $|U_{min}| = 1.3\varepsilon$ [lipid density = 3.048 lipid/nm^2].

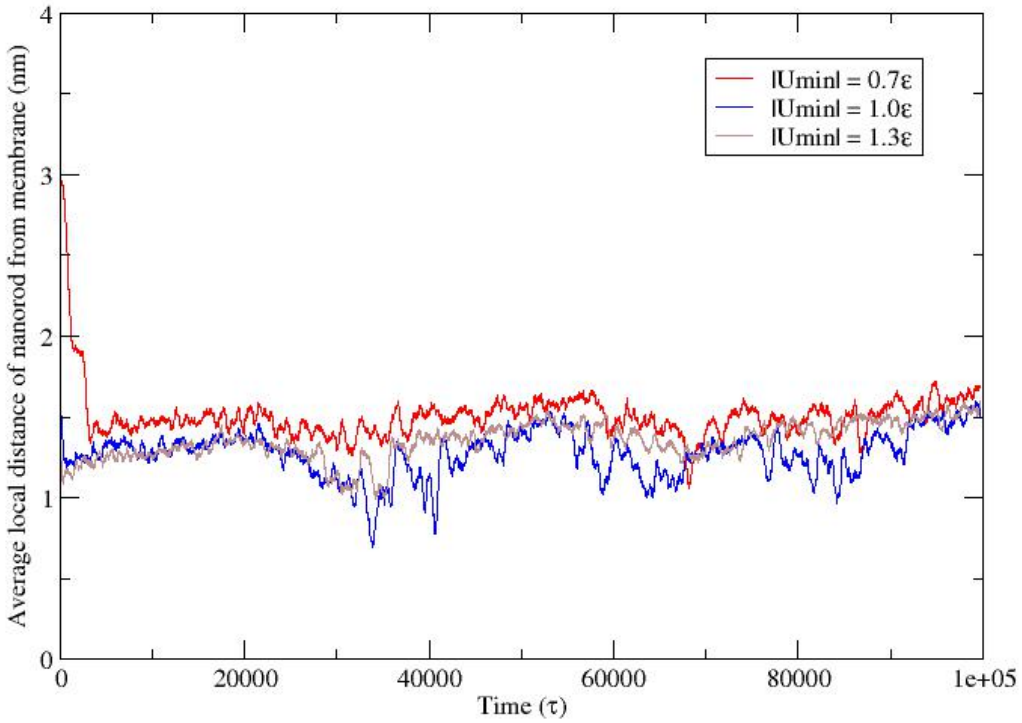

Figure 3.1.8. The time evolution of average local distance between nanorods and lipid membrane at constant area simulation of 7 nanorods (D = 2.76 nm, H = 5.52 nm) interacting with membrane at (i) $|U_{min}| = 0.7\varepsilon$ (ii) $|U_{min}| = 1.0\varepsilon$ and (iii) $|U_{min}| = 1.3\varepsilon$ [lipid density = 3.048 lipid/nm^2].

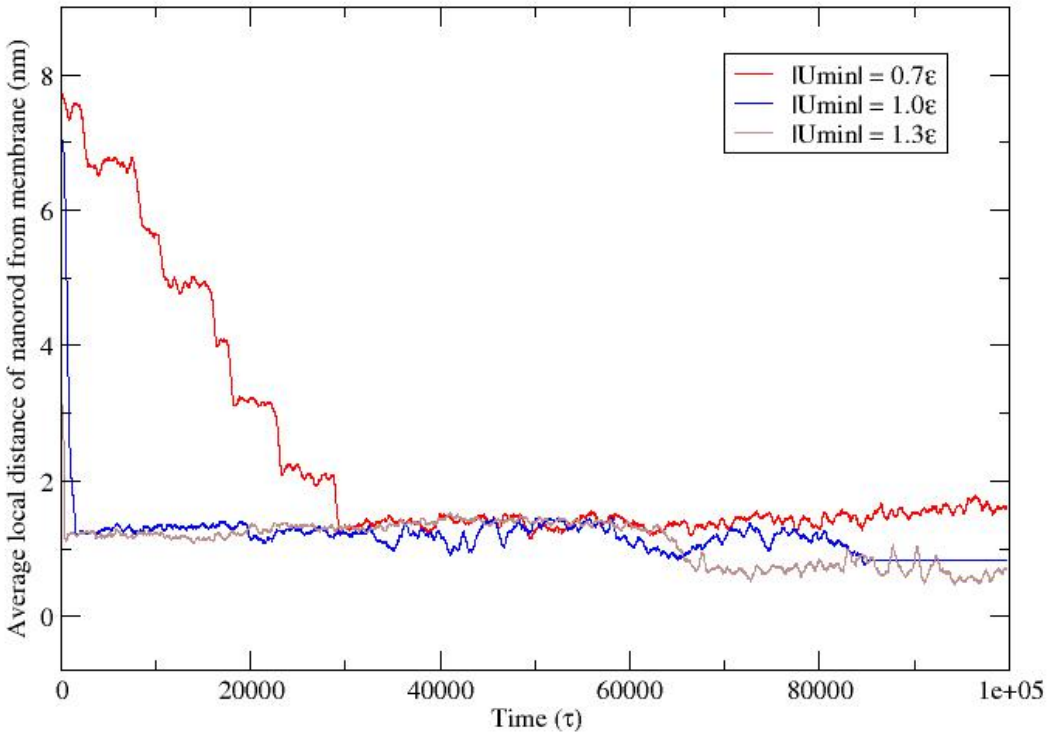

Figure 3.1.9. The time evolution of average local distance between nanorods and lipid membrane at constant area simulation of 7 nanorods (D = 2.76 nm, H = 13.80 nm) interacting with membrane at (i) $|U_{min}| = 0.7\varepsilon$ (ii) $|U_{min}| = 1.0\varepsilon$ and (iii) $|U_{min}| = 1.3\varepsilon$ [lipid density = 3.048 lipid/nm^2].

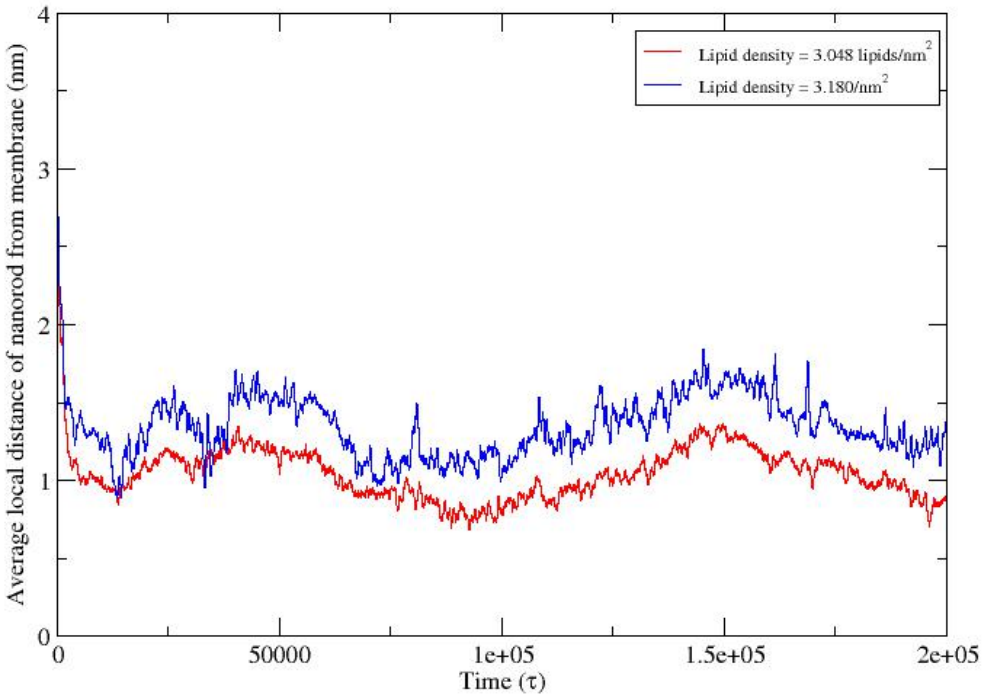

Figure 3.1.10. The time evolution of average local distance between nanorods and lipid membrane at constant area simulation of 20 nanorods (D = 2.76 nm, H = 5.52 nm) interacting with membrane at $|U_{min}| = 0.7\varepsilon$ [At lipid densities = 3.048 lipid/nm^2 and 3.180 lipid/nm^2].

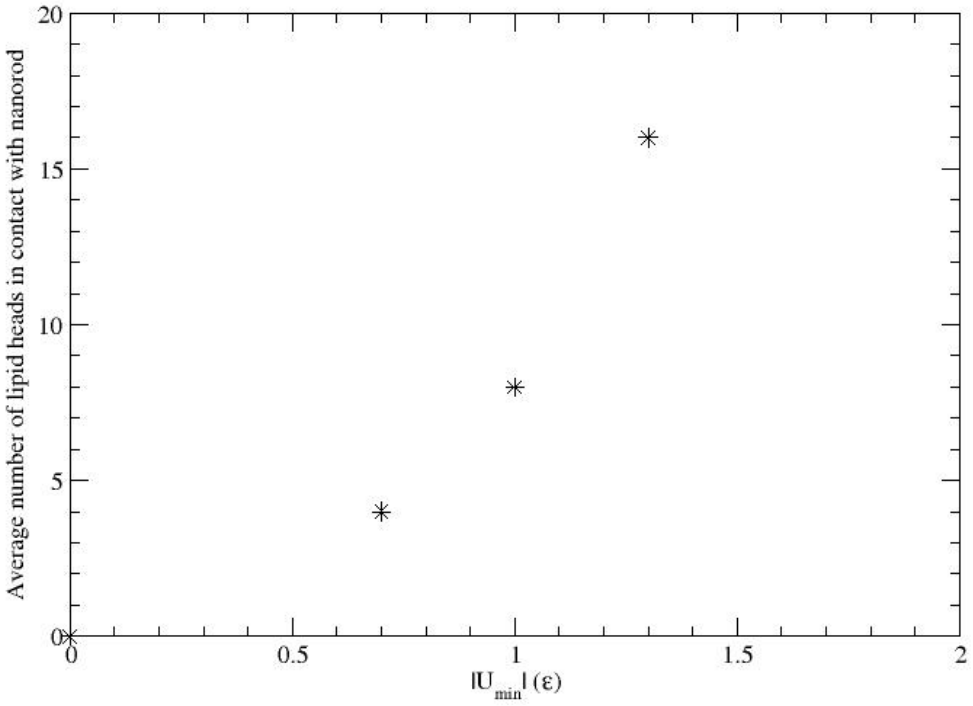

Figure 3.1.11. Average number of lipid heads in contact with nanorods at various nanorod-lipid head interactions ($|U_{min}| = 0.7\varepsilon$, 1.0ε and 1.3ε) for constant area simulation of 20 nanorods (D = 2.76 nm, H = 5.52 nm) [lipid density = 3.048 lipid/nm^2].

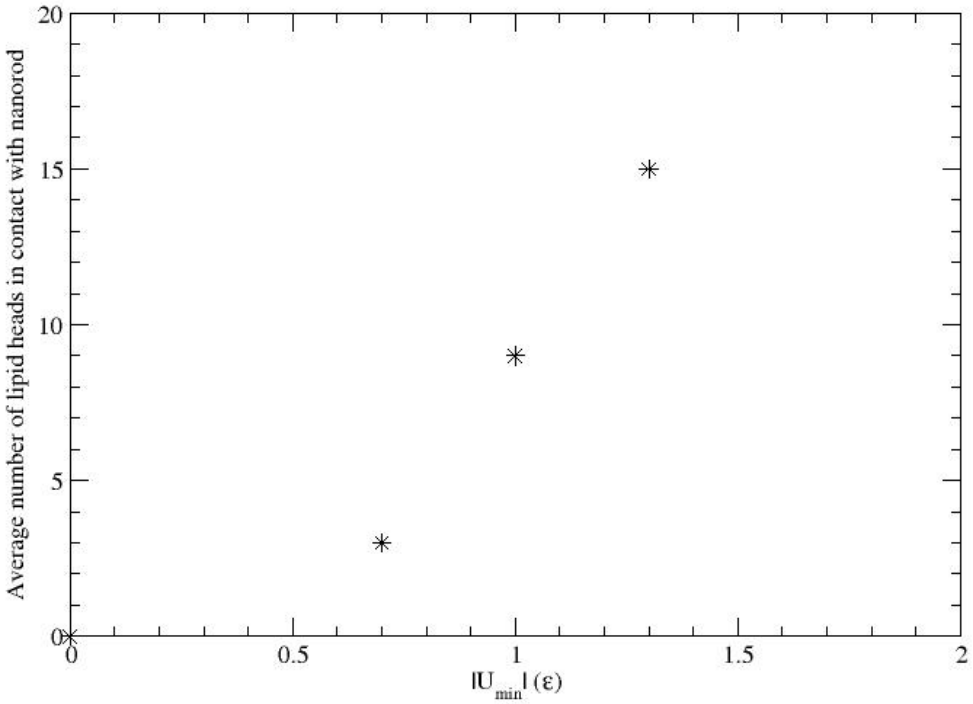

Figure 3.1.12. Average number of lipid heads in contact with nanorods at various nanorod-lipid head interactions ($|U_{min}| = 0.7\varepsilon$, 1.0ε and 1.3ε) for constant area simulation of 7 nanorods (D = 2.76 nm, H = 5.52 nm) [lipid density = 3.048 lipid/nm^2].

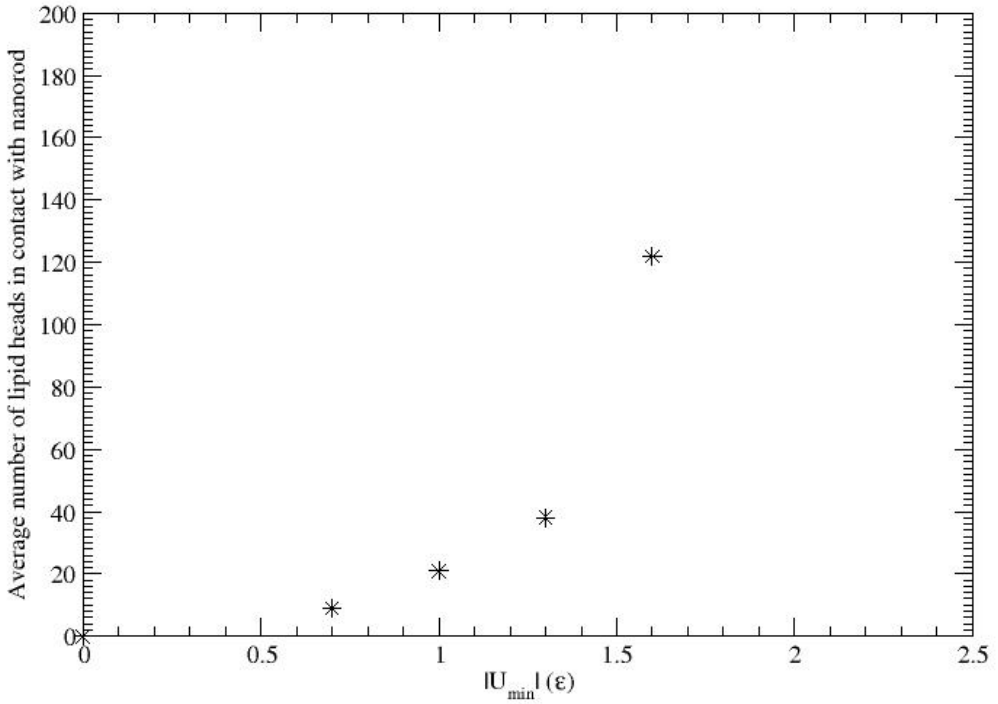

Figure 3.1.13. Average number of lipid heads in contact with nanorods at various nanorod-lipid head interactions ($|U_{min}| = 0.7\varepsilon$, 1.0ε, 1.3ε and 1.6ε) for constant area simulation of 7 nanorods (D = 2.76 nm, H = 13.80 nm) [lipid density = 3.048 lipid/nm^2].

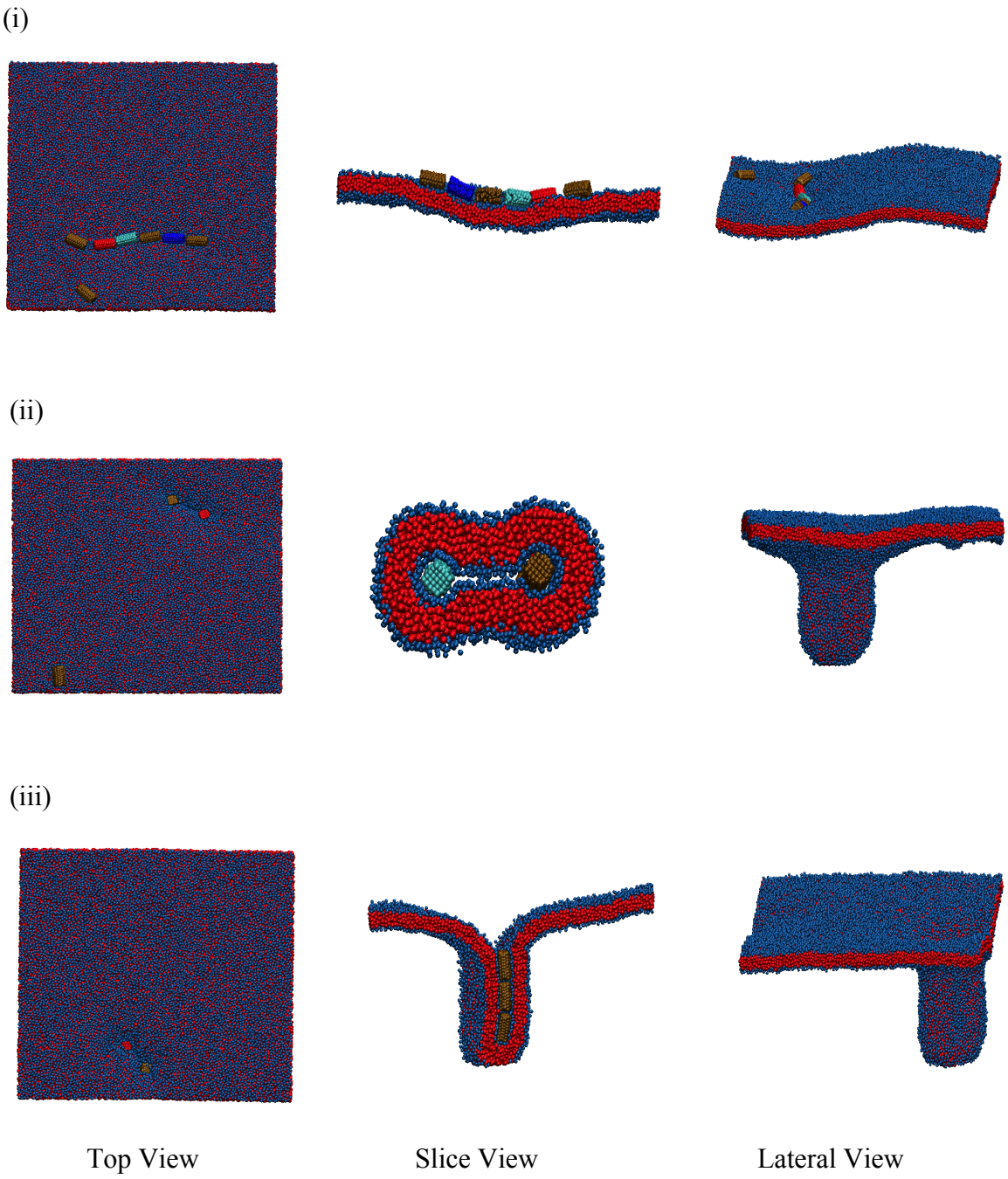

Figure 3.1.14. Snapshot of different views of 7 nanorods (D = 2.76 nm, H = 5.52 nm) interacting with membrane at (i) $|U_{min}| = 0.7\varepsilon$ (ii) $|U_{min}| = 1.0\varepsilon$ and (iii) $|U_{min}| = 1.3\varepsilon$ (constant pressure simulation).

(i)

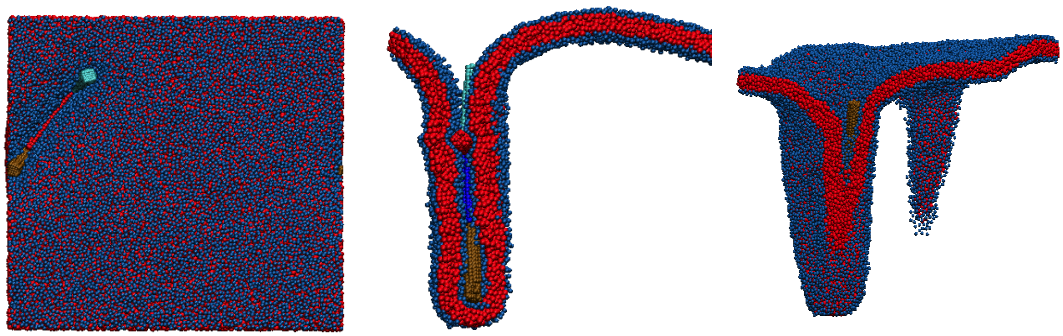

(ii)

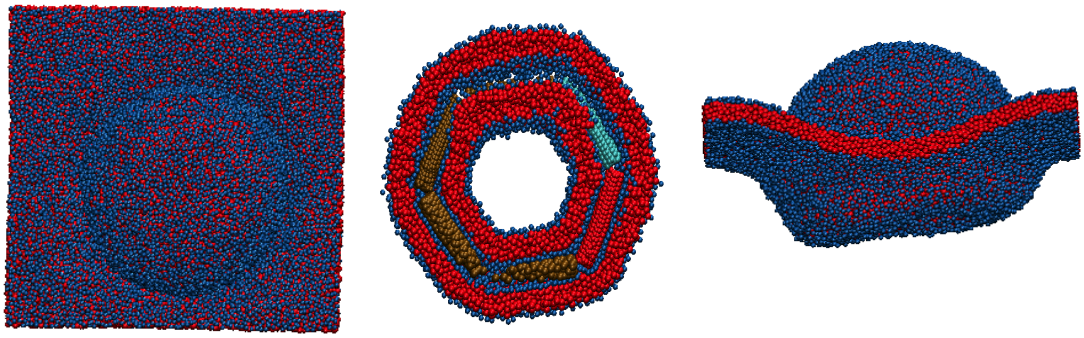

Top View Slice View Lateral View

Figure 3.1.15. Snapshot of different views of 7 nanorods (D = 2.76 nm, H = 13.80 nm) interacting with membrane at (i) $|U_{min}| = 0.7\varepsilon$ and (ii) $|U_{min}| = 1.0\varepsilon$ (constant pressure simulation).

(i)

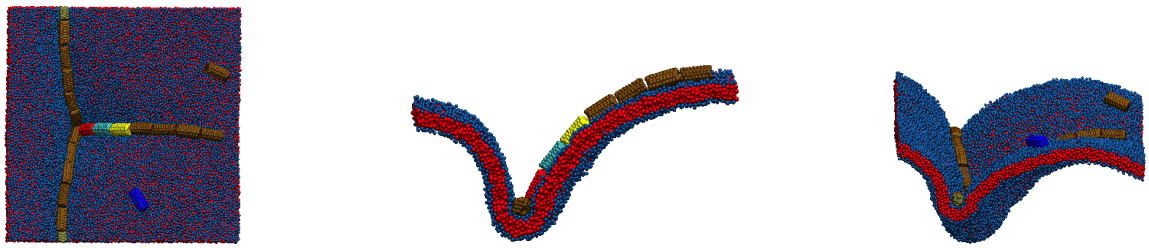

(ii)

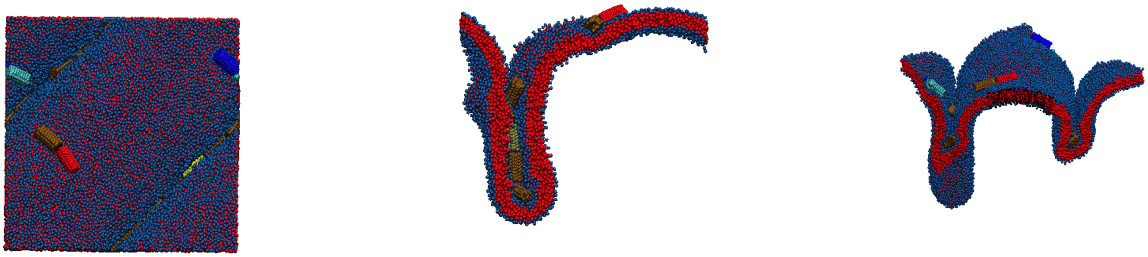

(iii)

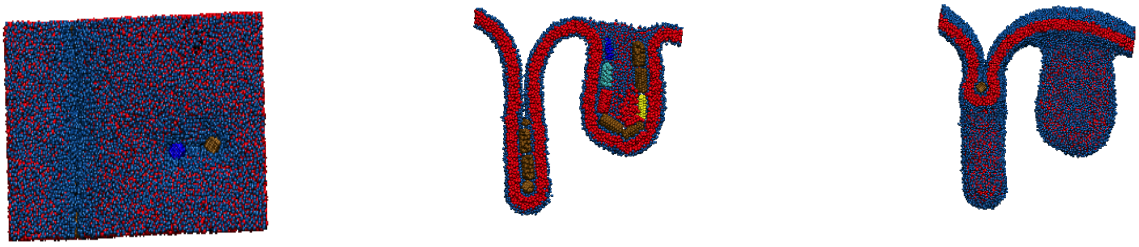

Top View Slice View Lateral View

Figure 3.1.16. Snapshot of different views of 20 nanorods (D = 2.76 nm, H = 5.52 nm) interacting with membrane at (i) $|U_{min}| = 0.7\varepsilon$, (ii) $|U_{min}| = 1.0\varepsilon$ and (iii) $|U_{min}| = 1.3\varepsilon$ (constant pressure simulation).

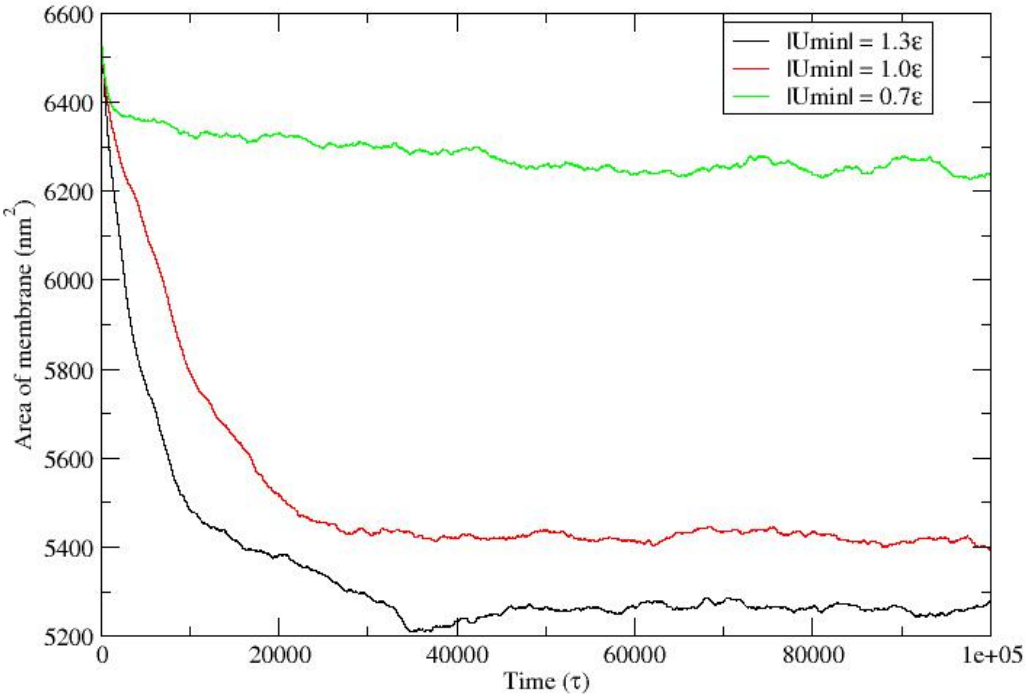

Figure 3.1.17. The time evolution of area of lipid membrane at constant pressure simulation of 7 nanorods (D = 2.76 nm, H = 5.52 nm) interacting with membrane at $|U_{min}|$ = 0.7ε, 1.0ε and 1.3ε.

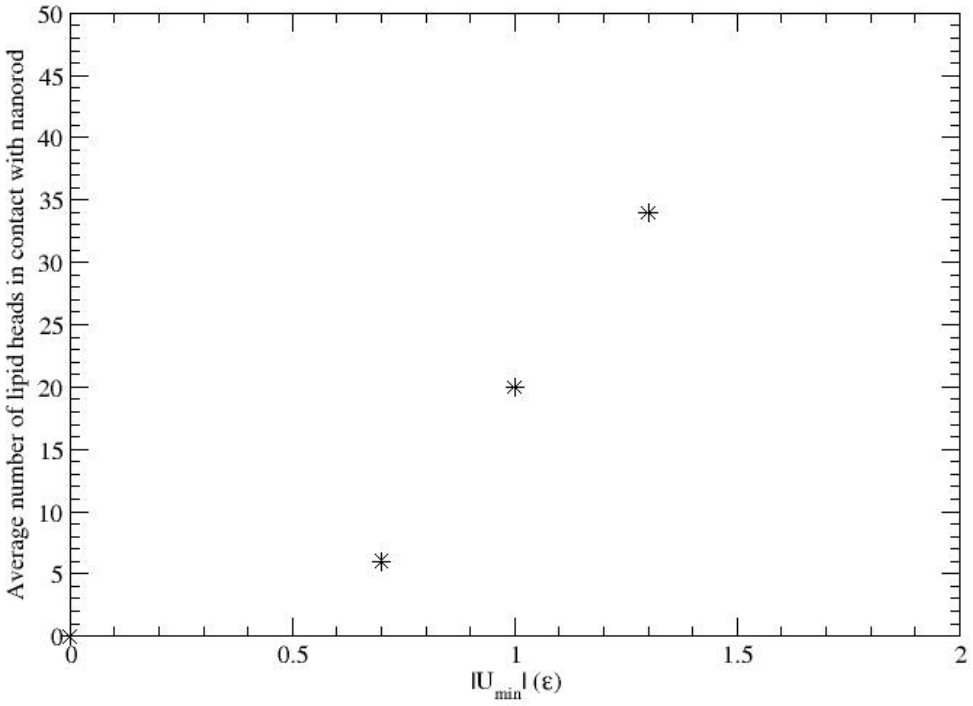

Figure 3.1.18. Average number of lipid heads in contact with nanorods at various nanorod-lipid head interactions ($|U_{min}| = 0.7\varepsilon$, 1.0ε and1.3ε) for constant pressure simulation of 7 nanorods (D = 2.76 nm, H = 5.52 nm).

3.2 Nanorod Internalization via Endocytosis

Understanding of endocytosis phenomenon of nanoparticles is crucial for drug delivery as well as to understand their potential cyto-toxic effects. The nanoparticles uptake by cells may depend upon their size. Although not directly observed, size dependent endocytosis of spherical nanoparticle is reported in computational research.[23,3] Endocytosis of ligand-coated nanoparticles is also reported.[24] In the current simulation, single nanorods (D =5.52 nm, H = 5.52 nm) are found to internalize at nanorod-lipid head interaction ($|U_{min}|$) = 1.0ε as shown in figure 3.2.1. Same kind of phenomenon is also observed with single nanorod (D = 5.52 nm, H = 13.80 nm) but at a lower value of interaction i.e. $|U_{min}|$ = 1.0ε as shown in figure 3.2.2. The results also indicate if the length of nanorod increases, endocytosis occurs at lower value interaction and even more quickly. Below these values of interaction where endocytosis take place, nanorods are embedded inside the membrane and beyond those values, short-lived pores are formed in the vicinity of the nanorods. The time evolution of area of lipid membrane shown in figure 3.2.3 demonstrates that an equilibrium state has been reached in my simulation.

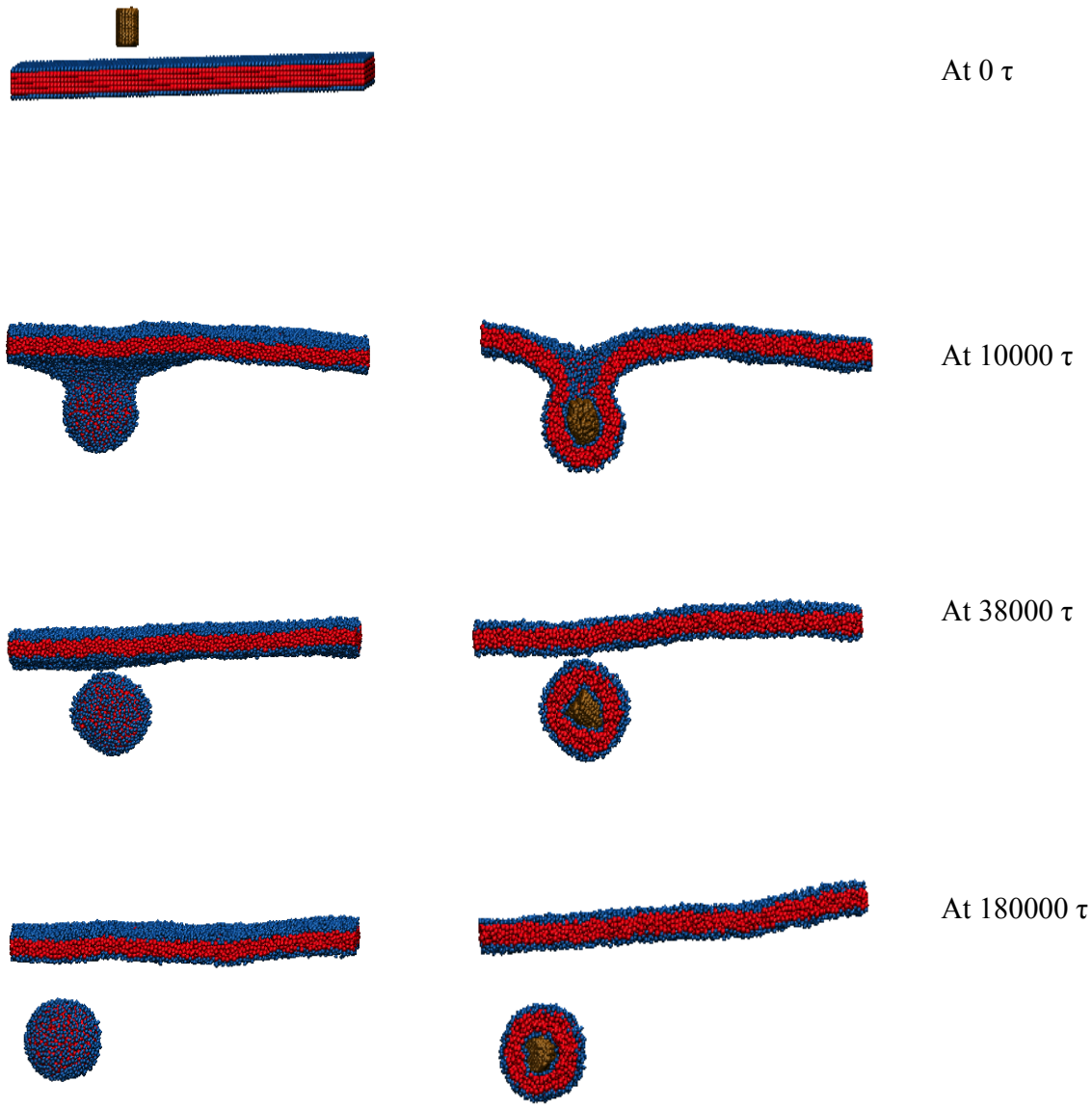

Figure 3.2.1. Snapshot sequence showing endocytosis of a single nanorod (D = 5.52 nm, H = 5.52 nm) through membrane at nanorod-lipid interaction $|U_{min}| = 1.3\varepsilon$ and at zero tension.

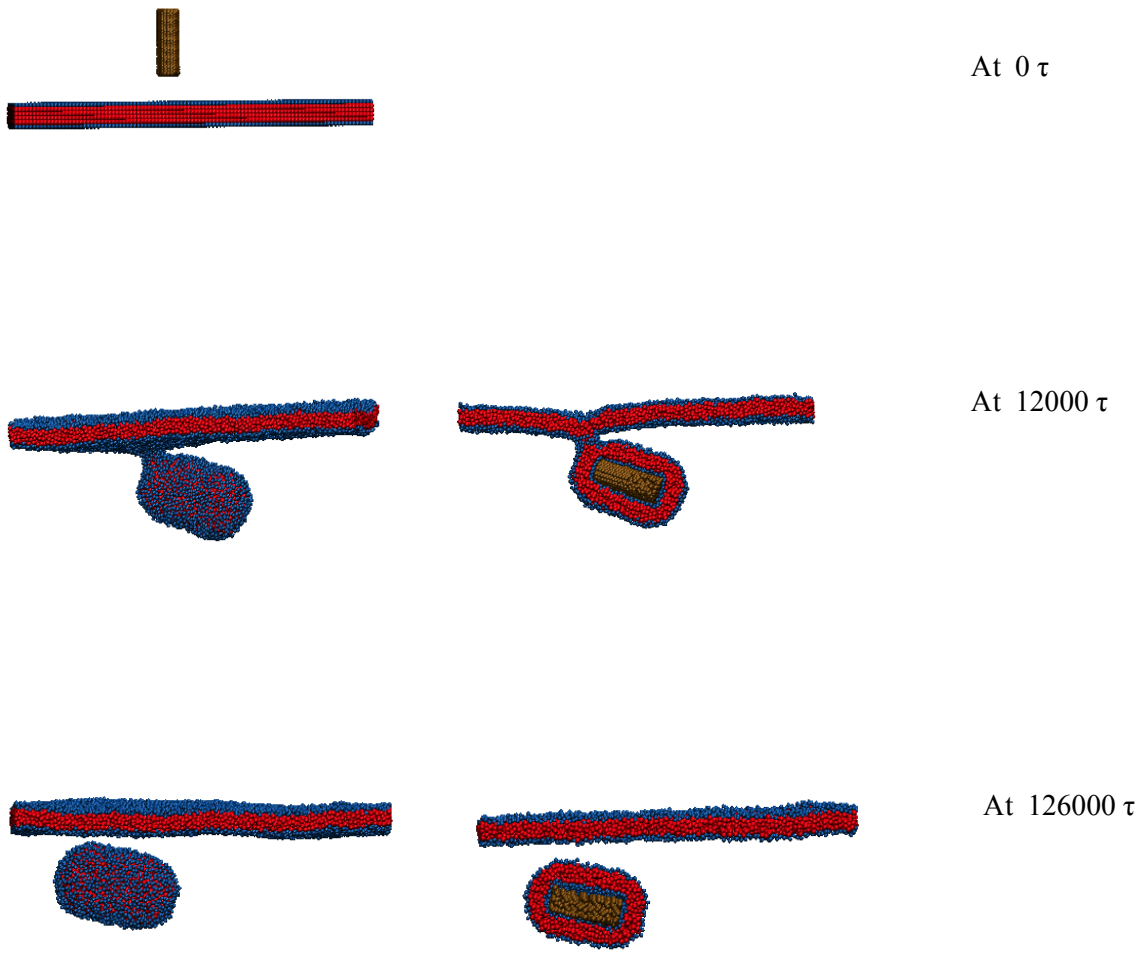

Figure 3.2.2. Snapshot sequence showing endocytosis of a single nanorod (D = 5.52 nm, H = 13.80 nm) through membrane at nanorod-lipid interaction $|U_{min}| = 1.0\varepsilon$ and at zero tension simulation.

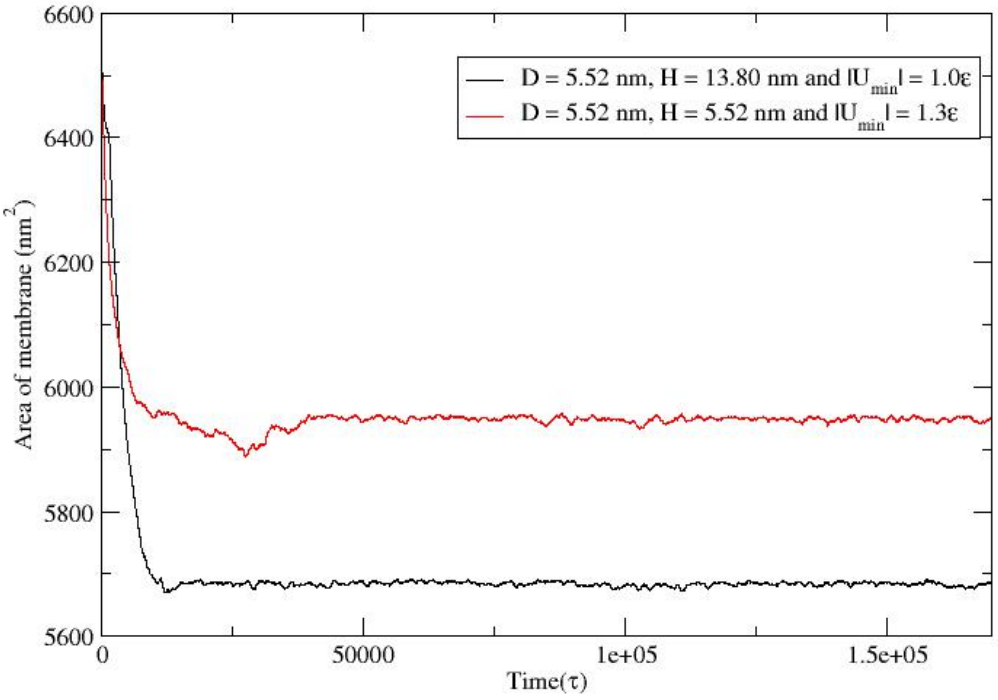

Figure 3.2.3. Time evolution of area of lipid membrane at zero tension simulation of a single nanorod (D = 5.52 nm, H = 5.52 nm and H = 13.80 nm) that internalizes via endocytosis.

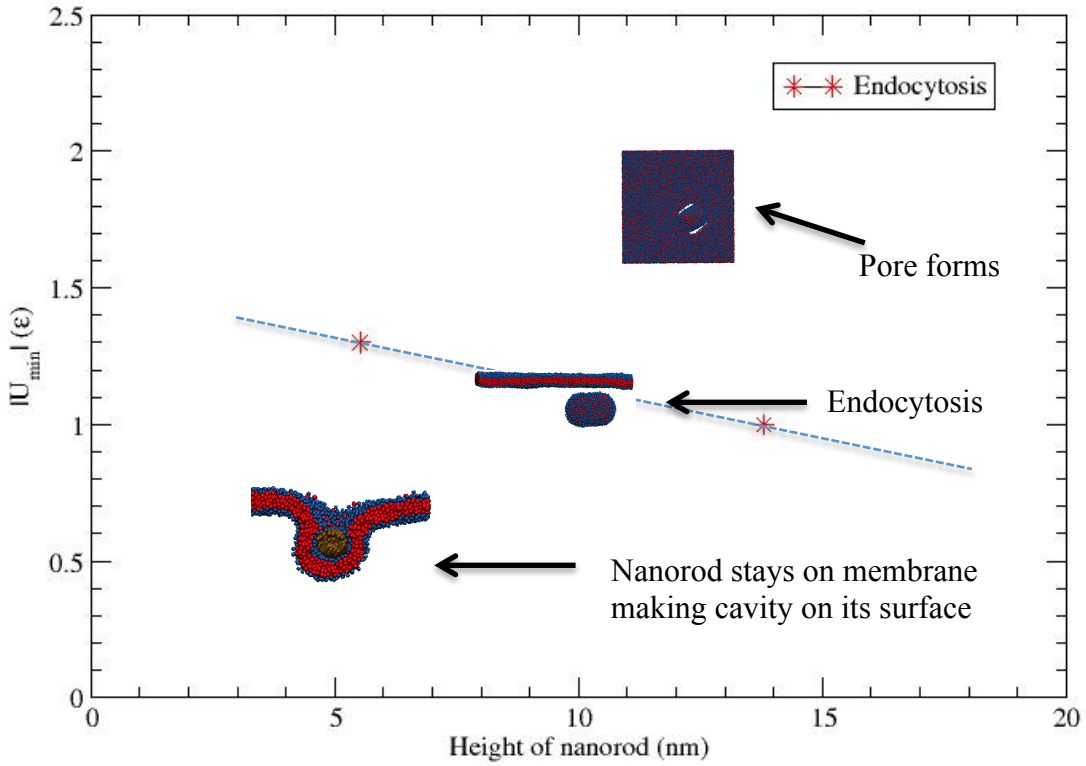

Figure 3.2.4. Preliminary phase diagram for zero tension simulation of single nanorod (D = 5.52 nm, H = 5.52 nm and 13.80 nm).

3.3 Hydrophilic Pore Formation in The Membrane

It is presumed that the interaction of nanoparticles with lipid membrane may lead to pore formation. If a transient pore forms across the bilayer, it may facilitate the transport of drugs, ions and proteins etc. On the other hand, if the pore persists for a long time, it may cause cell death. In this present work, it is observed that an increase in nanorod-lipid head interaction result in pores in the membrane as shown in figure 3.3.1 - 3.3.3 and figure 3.3.5. Pores are also observed to be more prominent as the diameter of the nanorods is increased as shown in figure 3.3.7. Increase in nanorod-lipid head interaction as well as diameter of rod increases the membrane curvature bending energy. In order to lower that interfacial energy, pores are formed in the membrane. Sometimes what looks like stable pores are formed while usually these pores persist for some time and are ultimately resealed. Pores also lead to membrane destruction. Our results indicate that resealing of the membrane is found to depend on its surface coverage of nanorods. For 7 nanorods (D = 2.76 nm, H = 13.80 nm, constant pressure simulation at $|U_{min}| = 2.0$), pores are resealed as shown in figure 3.3.8 whereas in case of 20 nanorods (D = 5.52 nm, H = 5.52 nm, constant pressure simulation at $|U_{min}| = 1.3$), pores lead to membrane destruction as shown in figure 3.3.9. Regarding pore formation, our conclusion is that membrane lysis occurs at higher concentration of nanorods or in the presence of thicker nanorods.

(i)

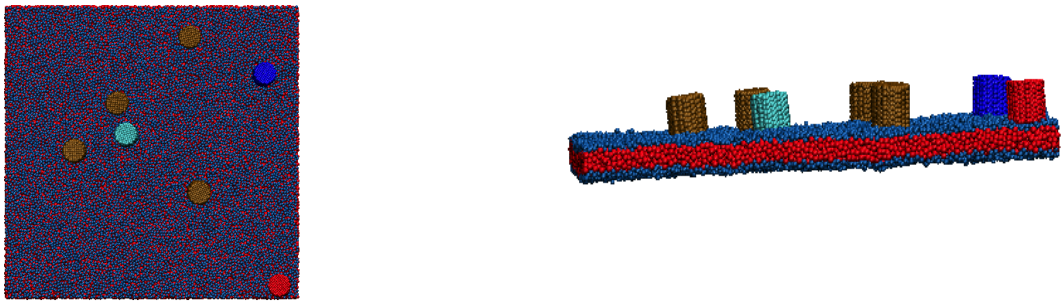

(ii)

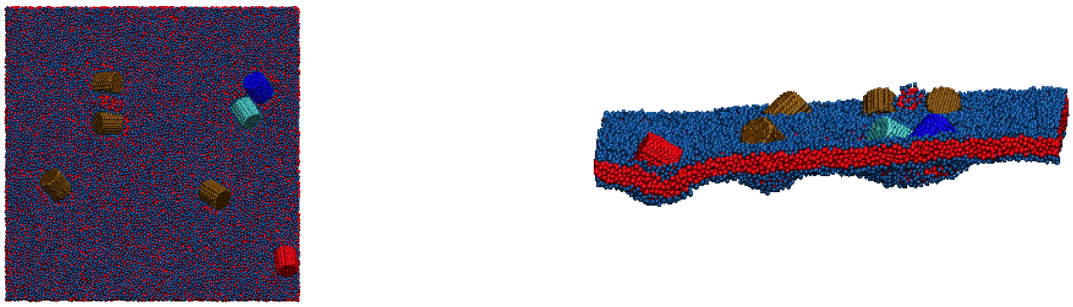

(iii)

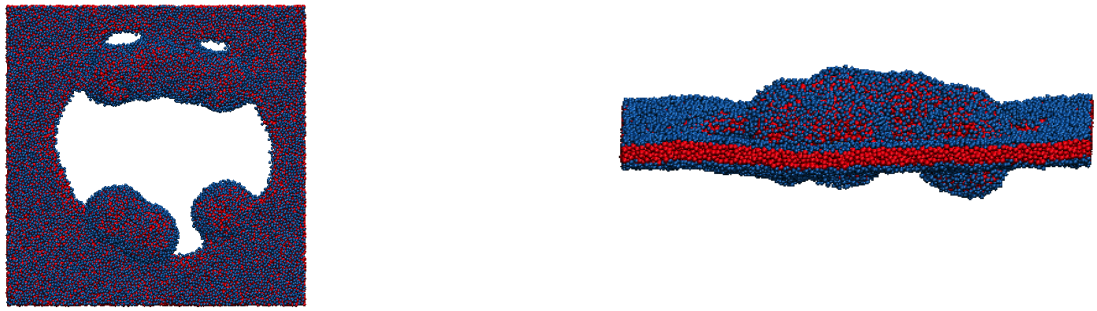

Top View Lateral View

Figure 3.3.1. Snapshot of different views of 7 nanorods (D = 5.52 nm, H = 5.52 nm) interacting with membrane at (i) $|U_{min}| = 0.7\varepsilon$ and (ii) $|U_{min}| = 1.0\varepsilon$ and (iii) $|U_{min}| = 1.3\varepsilon$ (lipid density = 3.048 lipids/nm^2).

(i)

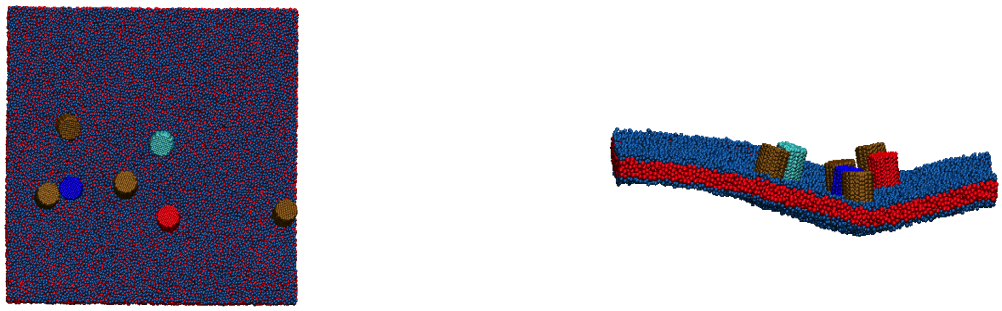

(ii)

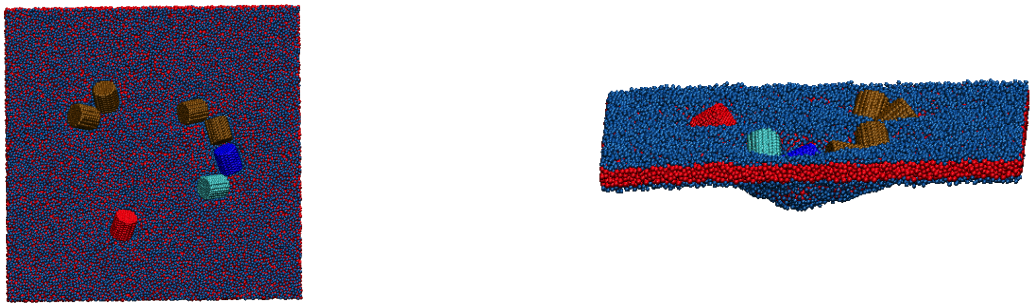

(iii)

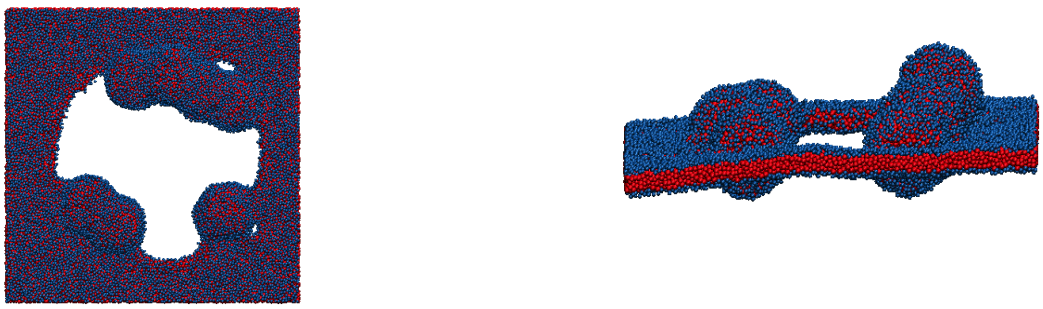

Top View Lateral View

Figure 3.3.2. Snapshot sequences of different views of 7 nanorods (D = 5.52 nm, H = 5.52 nm) interacting with membrane at (i) $|U_{min}| = 0.7\varepsilon$ and (ii) $|U_{min}| = 1.0\varepsilon$ and (iii) $|U_{min}| = 1.3\varepsilon$ (lipid density = 3.180 lipids/nm^2).

(i)

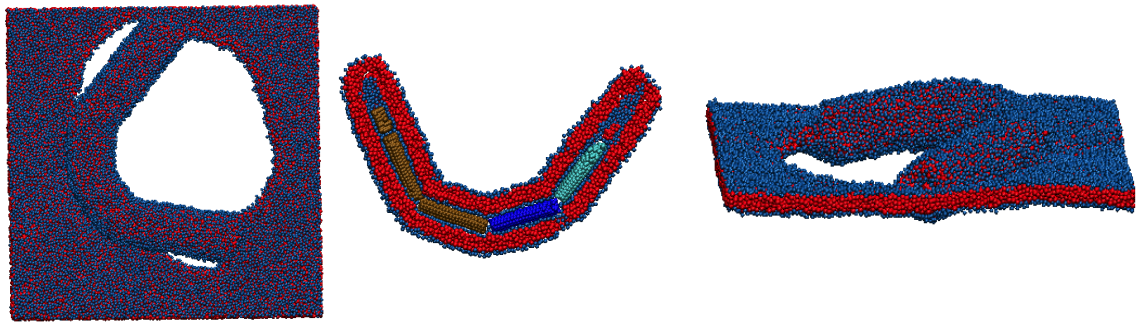

(ii)

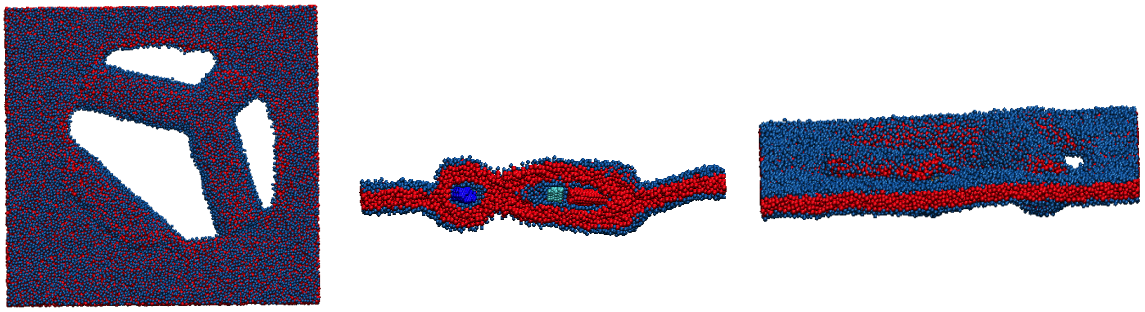

Top View Slice View Lateral View

Figure 3.3.3. Snapshot sequences of different views of 7 nanorods (D = 2.76 nm, H = 13.80 nm) interacting with membrane of (i) lipid density = 3.048 lipids/nm^{2}and (ii) lipid density = 3.180 lipids/nm^2 at $|U_{min}| = 1.6\varepsilon$.

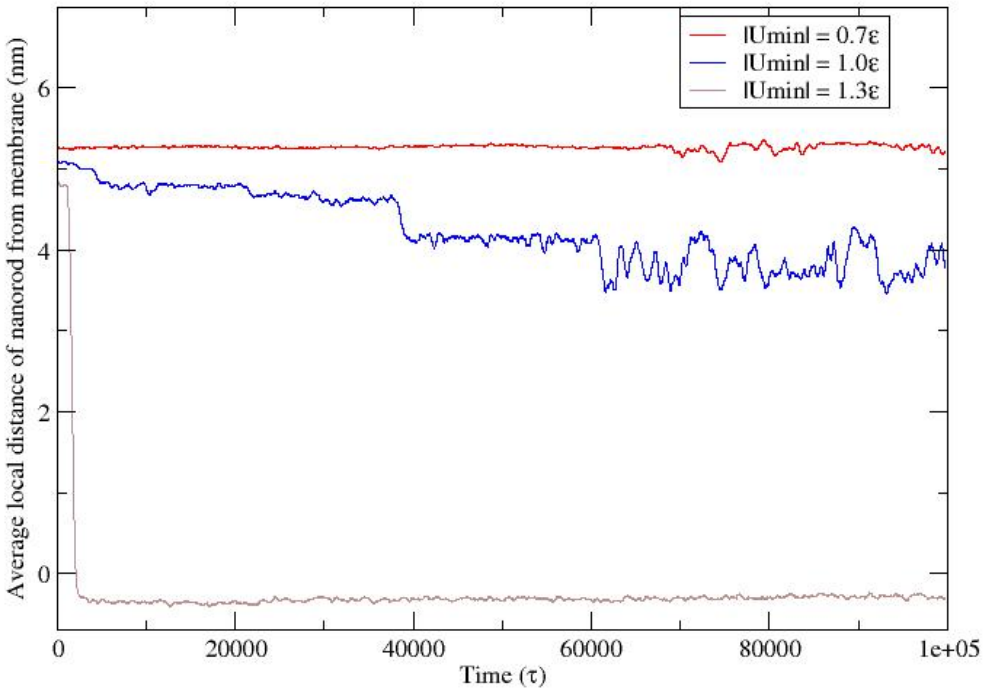

Figure 3.3.4. Time evolution of average local distance between nanorods and lipid membrane at constant area simulation of 7 nanorods (D = 5.52 nm, H = 5.52 nm) interacting with membrane at (i) $|U_{min}| = 0.7\varepsilon$ (ii) $|U_{min}| = 1.0\varepsilon$ and (iii) $|U_{min}| = 1.3\varepsilon$ [lipid density = 3.048 lipid/nm^2].

(i)

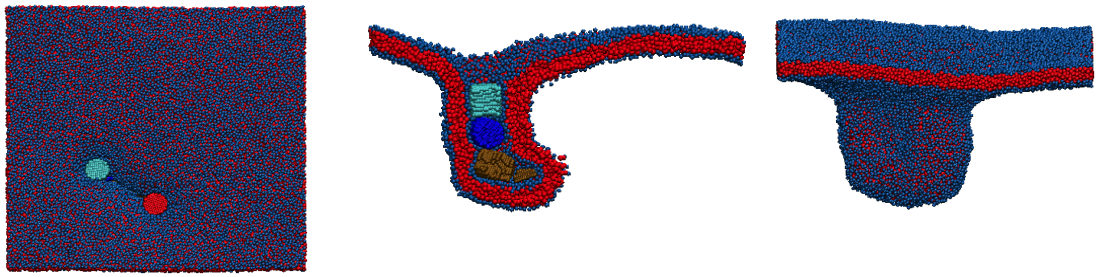

(ii)

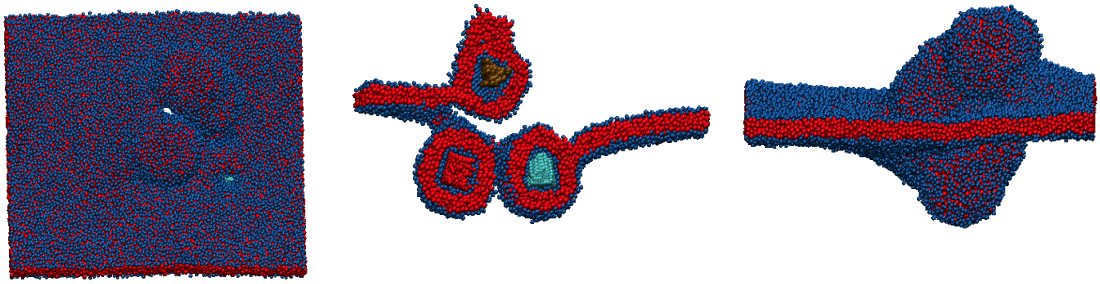

(iii)

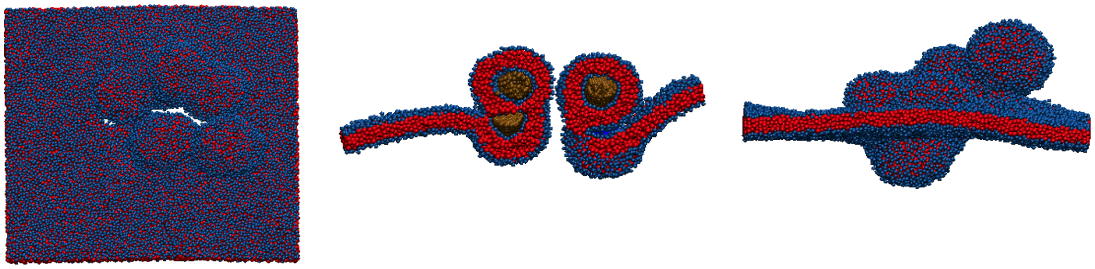

Top View Slice View Lateral View

Figure 3.3.5. Snapshot of different views of 7 nanorods (D = 5.52 nm, H = 5.52 nm) interacting with membrane at (i) $|U_{min}| = 0.7\varepsilon$ and (ii) $|U_{min}| = 1.0\varepsilon$ and (iii) $|U_{min}| = 1.3\varepsilon$ (constant pressure simulation).

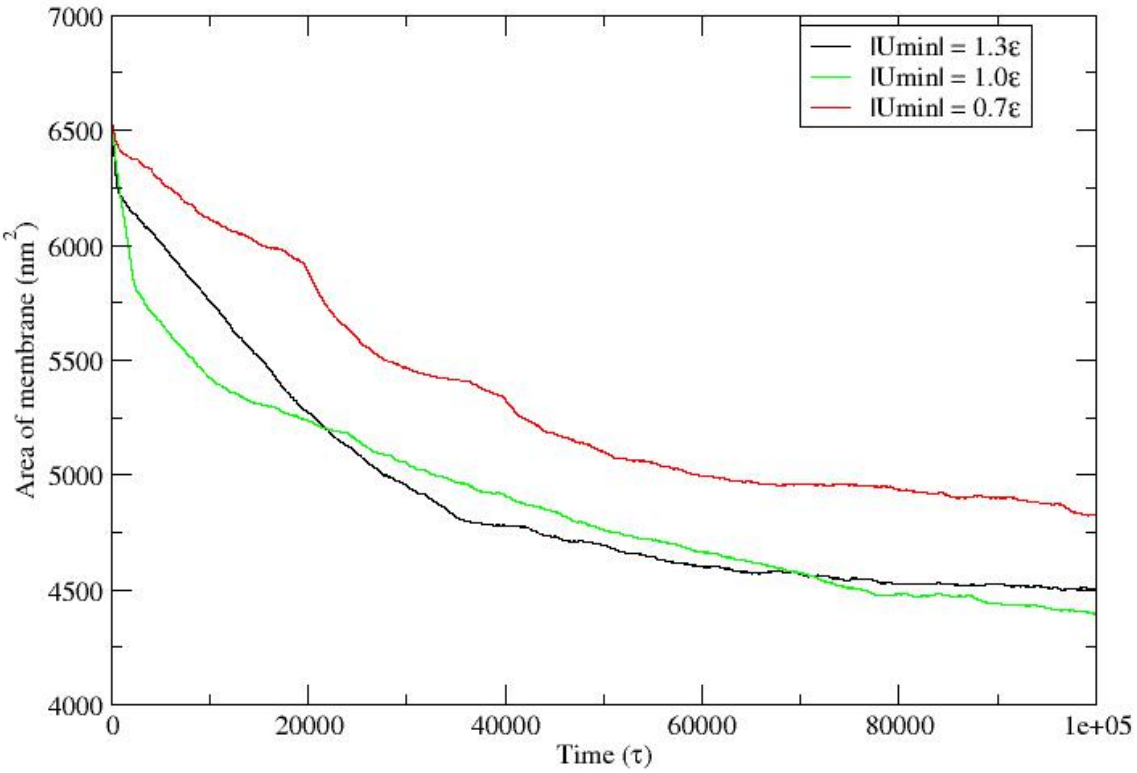

Figure 3.3.6. Time evolution of area of lipid membrane at constant pressure simulation of 7 nanorods (D = 5.52 nm, H = 5.52 nm) interacting with membrane at $|U_{min}| = 0.7\varepsilon$, 1.0ε and 1.3ε.

(i)

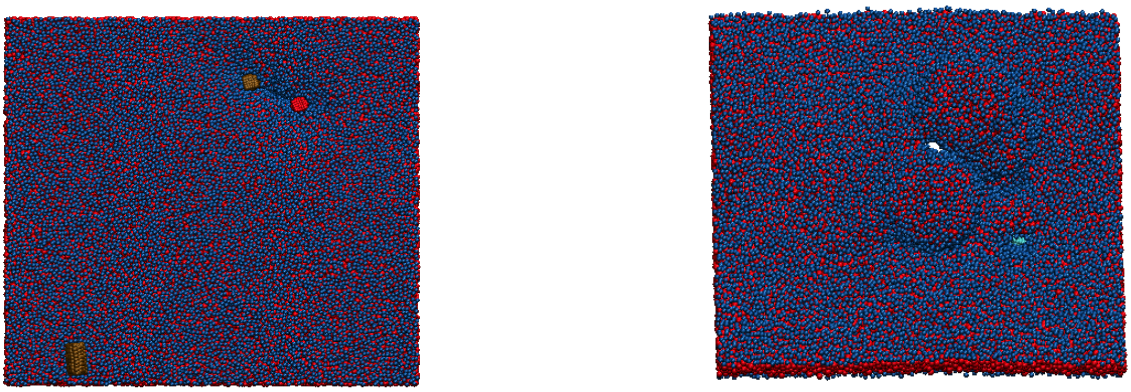

(ii)

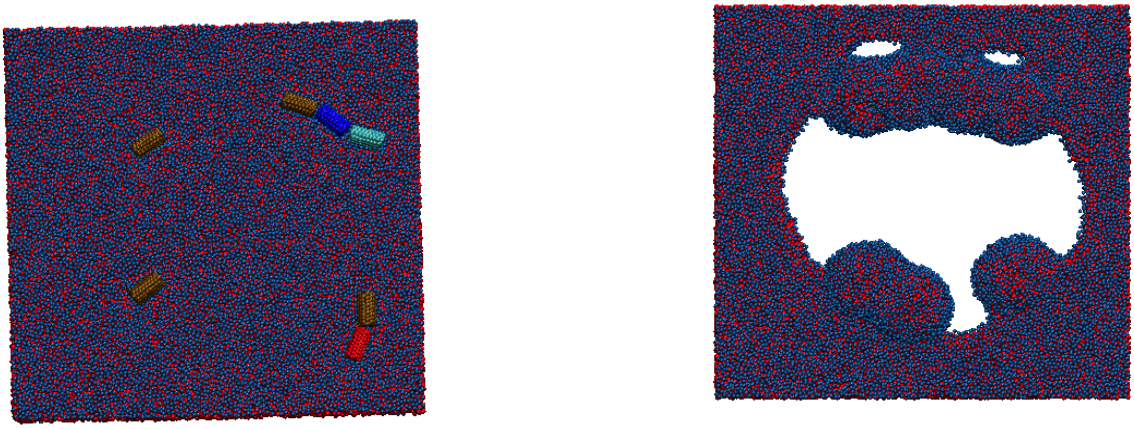

Figure 3.3.7. Snapshot sequences showing that increase in diameter of nanorods causes pore formation in the membrane at same interaction $|U_{min}| = 1.3\varepsilon$ (in above figure, on left: 7 nanorods, D = 2.76 nm, H = 5.52 nm and on right: 7 nanorods, D = 5.52 nm, H = 5.52 nm). (i) constant pressure simulation (ii) constant area simulation with lipid density = 3.048 lipids/nm^2.

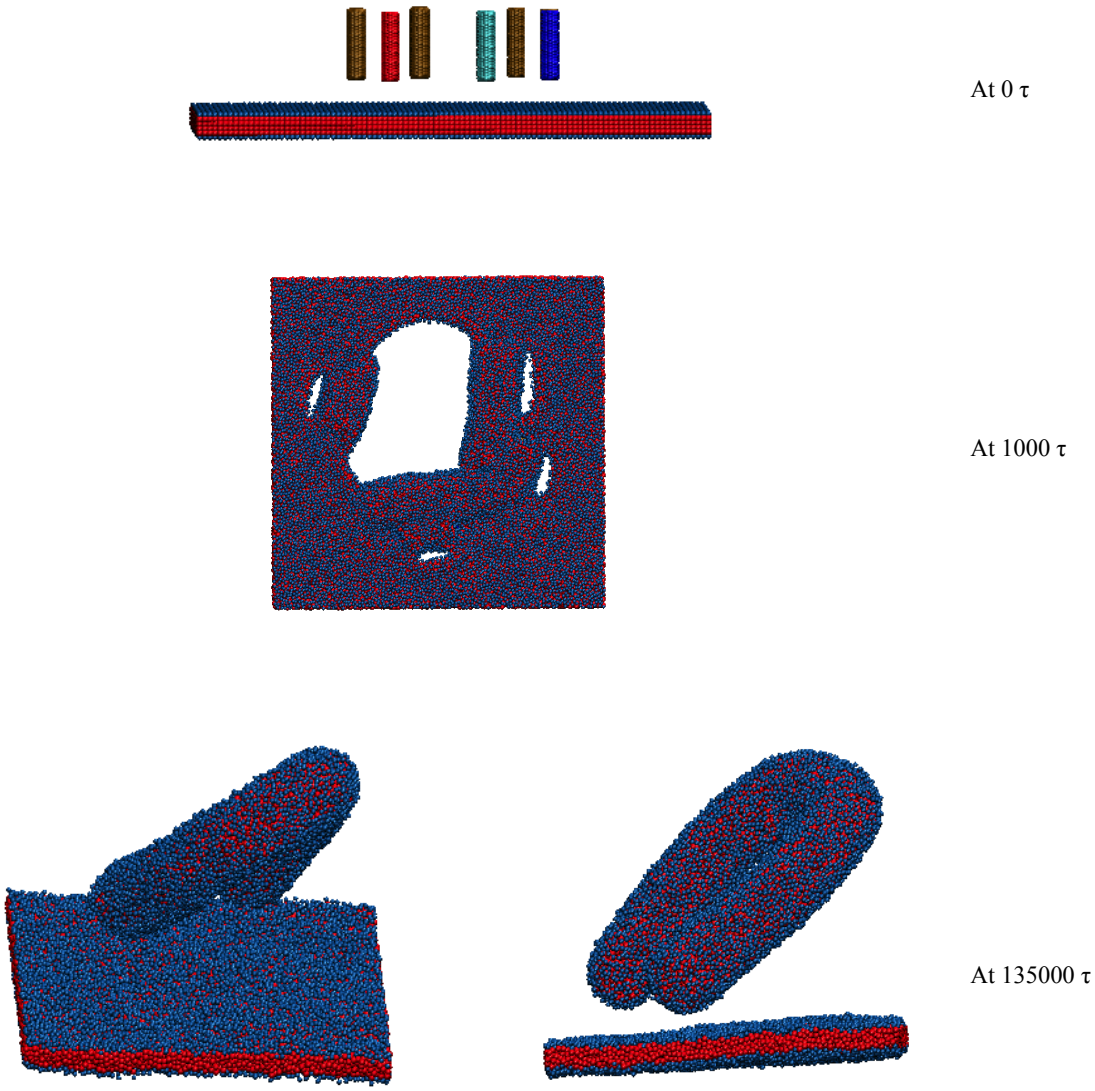

Figure 3.3.8. Snapshot sequences showing a time evolution of zero tension simulation of 7 nanorods (D = 2.76 nm, H = 13.80 nm) interacting with a bilayer at $|U_{min}| = 2.0\varepsilon$.

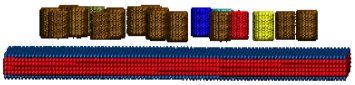

At 0 τ

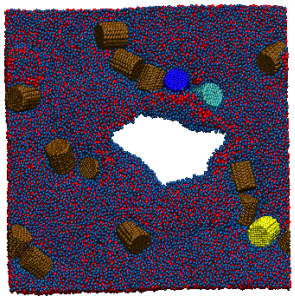

At 9000 τ

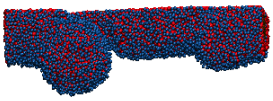

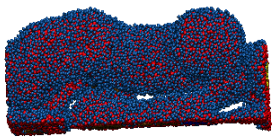

At 79000 τ

Figure 3.3.9. Snapshot sequences showing a time evolution of 20 nanorods (D = 2.76 nm, H = 5.52 nm) interacting with membrane at $|U_{min}| = 1.3\varepsilon$ at zero tension.

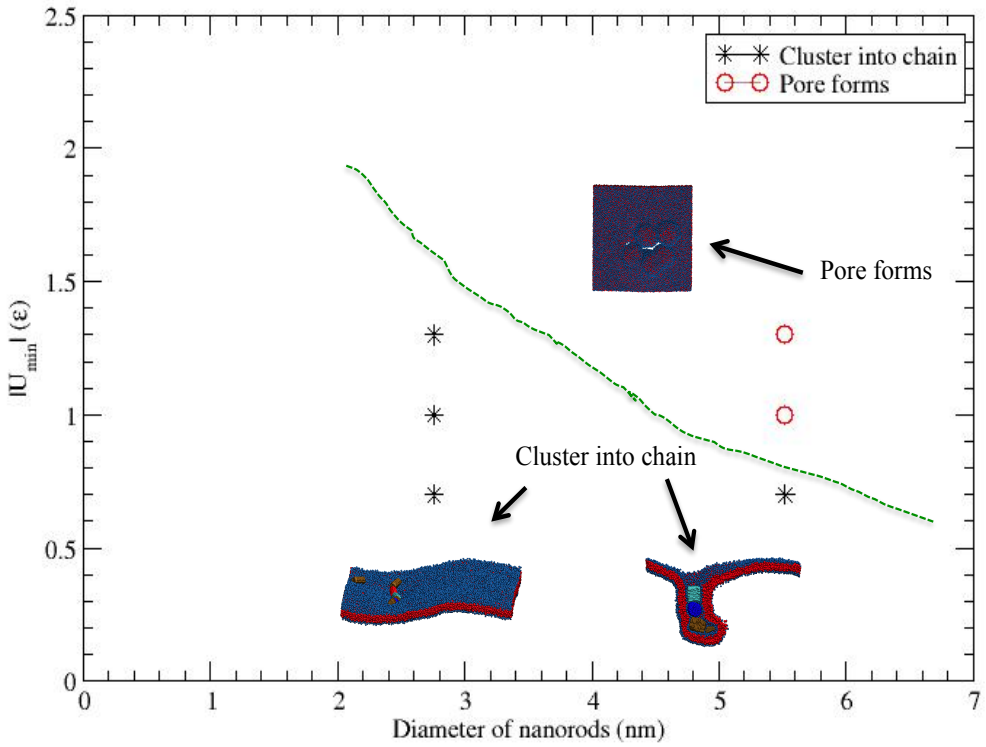

Figure 3.3.10. Preliminary phase diagram for constant pressure simulation of 7 nanorods (D = 2.76 nm and 5.52 nm, H = 5.52 nm).

Chapter 4

Conclusion

In this thesis, we studied the interactions of nanorods with lipid bilayer as a function of nanorod-lipid head interaction, size and their surface coverage. In particular we investigated the morphological changes of the lipid membranes and the internalization process of the nanoparticles. Our study is based on an implicit-solvent model for lipid bilayers recently developed by my group.

To investigate the effects of nanorod-lipid head interactions, we assigned different values of interactions ranging from $|U_{min}| = 0.7$ to 2.0. Our constant pressure and constant area simulation results showed that moderate values of $|U_{min}|$ leads to clustering of the nanorods into chains without touching each other. Further increase in the interaction potential led to membrane lysis.

Size-dependent interactions were also studied carefully. Depending on their size, nanorods adsorption on the membrane can induce pores in the membrane. In contrast to thinner nanorods (D = 2.76 nm), thicker nanorods (D = 5.52 nm) produce pores in the lipid bilayer even at lower values of nanorod-lipid interaction. Furthermore, size dependency was also significant in the internalization process of single nanorods across the membrane. Increasing the length of thicker nanorods is found to lower the threshold value of the nanorod-lipid interaction for the endocytosis process. That is, length of rod has inverse relationship with nanorod-lipid interaction.

Additionally, the adverse effect of surface coverage was also observed during the simulations. Increase in nanoparticles' density increases the surface coverage on the membrane that ultimately leads to membrane destruction.

In this research, nanoparticles interact with the membrane via soft interactions, but most of the times, nanoparticles are transported to the targeted drug delivery sites and tumor sites using some form of force, which may be chemical or physical in nature. So, interaction between nanoparticles and lipid membrane in which an external force is applied on the NPs is the next step in further understanding the interaction between the lipid membranes and the NPs.

Science and engineering community is always working towards optimizing the properties of materials by changing their shape and size for a more efficient and sometimes for a different application of the material. In that regard, hard nanoshells may have completely different properties and may induce a different effect on the membrane than nanorods. It would also be interesting to see how the lipid membranes interact with hollow cylindrical shells instead of cylindrical rods. Will we see pore formation in the membrane as we saw in the case of the nanorods? Will we see endocytosis of nanoshells? Will the membrane rupture completely? Working with the cylindrical nanoshells will help, in my opinion, to answer these important questions.

REFERENCES

(1) Buzea, C.; Pacheco, I.; Robbie, K. *Biointerphases* **2007**, *2*, 17-71.

(2) Nohynek, G. J.; Dufour, E. K. *Arch. Toxicol.* **2012**, *86*, 1063-1075.

(3) Chen, X.; Tian, F.; Zhang, X.; Wang, W. *Soft Matter* **2013**, DOI: 10.1039/C3SM50931A.

(4) Lovett, M.; Lee, K.; Edwards, A.; Kaplan, D. L. *Tissue Eng. Part B Rev.* **2009,** *15*, 353-370.

(5) Tiwari, P. M.; Vig, K.; Dennis, V. A.; Singh, S. R. *Nanomaterials* **2011**, *1*, 31-63.

(6) Ma, Y.; Nolte, R. J. M.; Cornelissen, J. J. L. *Adv. Drug Deliv.* **2012**, *64*, 811-825.

(7) Bruchez, M.; Moronne, M.; Gin, P.; Weiss, S.; Alivisatos, A. P. *Science* **1998**, *281*, 2013-2016.

(8) Edelstein, R. L.; Tamanaha, C. R.; Sheehan, P. E.; Miller, M. M.; Baselt, D. R.; Whitman, L. J.; Colton, R. J. *Biosens Bioelectron.* **2000**, *14*, 805-813.

(9) Xue, Z.; Liang, D.; Li, Y.; Long, Z.; Pan, D.; Liu, X.; Wu, L.; Zhu, S.; Cai, F.; Dai, H.; Tang, B.; Xia, K.; Xia, J. *Chin. Sci. Bull.* **2005**, *50*, 2323-2327.

(10) Sadhukha, T.; Wiedmann, T. S.; Panyam, J. *Biomaterials* **2013**, *34*, 5163-5171.

(11) Lee, S.; O'Halloran, T. V.; Nguyen, S. T. *J. Am. Chem. Soc.* **2010**, *132*, 17130-17138.

(12) Wang, S.; Lee, C.; Chiou, A.; Wei, P. *J. Nanobiotechnol* **2010**, *8*, 33.

(13) Raffi, M.; Hussain, F.; Bhatti, T. M.; Akhter, J. I.; Hameed, A.; Hasan, M. M. *J. mater. Sci. Technol.* **2008**, *24*, 92-96.

(14) Horie, M.; Kato, H.; Iwahashi, H. *Arch. Toxicol.* **2013**, *87*, 771-781.

(15) Biswas, P.; Wu, C. *J. Air Waste Manage. Assoc.* **2005**, *55*, 708-746.

(16) Lam, C.; James, J. T.; McCluskey, R.; Hunter, R. L. *Toxicol. Sci.* **2004**, *77*, 126–134.

(17) Zhao, Y.; Gu, X.; Ma, H.; He, X.; Liu, M.; Ding, Y. *J. Phys. Chem.* **2011**, *115*, 12797–12802.

(18) Liu, Y.; Zhao, Y.; Sun, B.; Chen, C. *Acc. Chem. Res.* **2013**, *46*, 702–713.

(19) Mouritsen, O. G. *Life-As a Matter of Fat*. 1st ed; Springer: New York, 2005; 1-52.

(20) Alberts, B.; Johnson, A.; Lewis, J.; Raff, M.; Roberts, K.; Walter, P.; Wilson, J.; Hunt, T. *Molecular Biology of The Cell*. 5th ed; Garland science: New York, 2008; 617-629.

(21) Revalee, J. D.; Laradji, M.; Sunil, P. B. *J. Chem. Phys.* **2008**, *128*, 035102.

(22) Roiter, Y.; Ornatska, M.; Rammohan, A. R.; Balakrishnan, J.; Heine, D. R.; Minko, S. *Nano Lett.* **2008**, *8*, 941–944.

(23) Lai, K.; Wang, B.; Zhang, Y.; Zheng, Y. *Phys. Chem. Chem. Phys.* **2013**, *15*, 270-278.

(24) Rocha, E. L.; Caramori, G. F.; Rambo, C. R. *Phys. Chem. Chem. Phys.* **2013**, *15*, 2282-2290.

(25) Li, Y.; Gu, N. *J. Phys. Chem.* **2010**, *114*, 2749–2754.

(26) Spangler, E. J.; Harvey, C. W.; Revalee, J. D.; Sunil, P. B.; Laradji, M. *Physical Review E* **2011**, *84*, 051906.

(27) Ercolessi, F. **1997**, retrieved from http://www.ud.infn.it/%7Eercolessi/md/md/md.html

(28) Grest, G. S.; Kremer, K. *Phys. Rev. A* **1986**, *33*, 3628–3631.

(29) Vattulainen, I.; Karttunen, M.; Besold, G.; Polson, J.M. *J. Chem. Phys.* **2002**, *116*, 3967-3979.

(30) Allen, M. P.; Tildesley, D. J. *Computer Simulation of Liquids.* 1st ed; Oxford: New York, 1987; 78-82.

(31) Saric, A.; Cacciuto, A. *Phys. Rev. Lett.* **2012**, *108*, 118101.